Enhancing Aerodynamic Performance of a Rotating Propeller Through CFD Design Optimisation

AEE3000 – Capstone Project [2024/2025 T1]

Student Name:	Tho Jia Qi
Student ID:	2202506
Degree Program:	BEng (Hons) Aerospace Engineering
Academic Supervisor:	Prof. Henrik Hesse
Date of Submission:	04 April 2025

ABSTRACT

This project investigates the aerodynamic optimisation of a quadcopter propeller using Computational Fluid Dynamics (CFD) with the Moving Reference Frame (MRF) approach. The study focuses on improving propeller performance under static hovering conditions, where accurate prediction of aerodynamic forces is critical. APC propellers (10x7" and 8x3.8") were first analysed using the MRF technique and validated against experimental wind tunnel data from the UIUC Propeller Database, ensuring the reliability of the simulation setup.

To explore geometry-based performance improvements, two design modifications were introduced to a baseline model: swept-back blades and downward winglets. These features were hypothesised to reduce tip vortex intensity and improve aerodynamic efficiency. The CFD simulations evaluated key performance parameters—including thrust, torque, and efficiency coefficients—as well as flow visualisation through velocity and pressure contours.

The swept-back design demonstrated enhanced thrust and smoother flow characteristics, while the downward winglet configuration yielded the highest thrust-to-torque ratio, indicating improved power efficiency. These results confirm the effectiveness of the MRF-based CFD framework in predicting aerodynamic behaviour and support the potential of tailored blade designs to enhance UAV hover efficiency.

ACKNOWLEDGEMENTS

I would like to express my sincere gratitude to Dr. Henrik Hesse, my academic supervisor, for his invaluable guidance, and insightful feedback throughout this project. His expertise in aerodynamics has greatly contributed to the successful execution and completion of this research.

Special thanks to Dr. Victor Wang for his support and for connecting me with Mr Sivamoorthy, an experienced researcher in CFD whose guidance was instrumental in helping me understand and apply the simulation methodology effectively.

I would also like to extend my appreciation to Mr Steven Chua, the laboratory technician of Lab SR8AB, for his assistance and for allowing me to run overnight CFD simulations in the lab. His support ensured the smooth operation and continuity of my simulation work.

Finally, I am grateful to my peers, friends, and family for their unwavering support throughout this project, and to Singapore Institute of Technology for providing the necessary resources and facilities that made this work possible.

TABLE OF CONTENTS

LIST OF FIGURES

LIST OF TABLES

NOMENCLATURE

Symbol	Description	Units
V_∞	Free-stream velocity	m/s
v	Velocity	m/s
w	Total induced acceleration	m/s^2
P_∞	Ambient pressure	Pa
$\dot{m}$	Mass flow rate	kg/s
A	Disc area	m^2
F_{fluid}	Force exerted by fluid	N
T	Thrust	N
$\dot{T}$	Power produced by propeller	W
P	Power required	W
C_T	Thrust coefficient	Dimensionless
C_Q	Torque coefficient	Dimensionless
C_P	Power coefficient	Dimensionless
ρ	Density	kg/m^3
n	Rotational speed	rev/s
D	Diameter	mm
Q	Torque	Nm
θ	Pitch angle	^{o}
φ	Flow angle	^{o}
α	Angle of attack	^{o}
ΔL	Differential lift force	N
C_L	Lift coefficient	Dimensionless
c	Chord length	mm
dr	Differential span wise length	mm
ΔD	Differential drag force	N
ΔQ	Incremental torque	Nm
H	Height	M
W	Width	M
J	Advance ratio	Dimensionless

LIST OF ABBREVIATION

Abbreviation	Description
UAV	Unmanned Aerial Vehicle
CFD	Computational Fluid Dynamics
MRF	Moving Reference Frame
CAD	Computed Aided Design
SST	Shear Stress Transport
AoA	Angle of Attack
BET	Blade Element Theory
LES	Large Eddy Simulation
DOE	Design of Experiments

1 INTRODUCTION

Unmanned Aerial Vehicles (UAVs) are gaining increasing population due to their advantages over manned flights. Their versatility enables their use across various sectors, including transport, search and rescue, military operations, surveillance, agriculture, and delivery (Mohsan et al., 2023) [1]. Furthermore, UAVs are cost-effective and require fewer resources to operate and maintain. In scenarios such as disaster response, firefighting, and hazardous material spills, they provide a safer alternative as they eliminate the risk to human lives. The global UAV market is anticipated to expand further over the next decade. Figure 1 illustrates the market value of UAVs in 2018 and the projected value by 2029, measured in billion United States Dollars (USD).

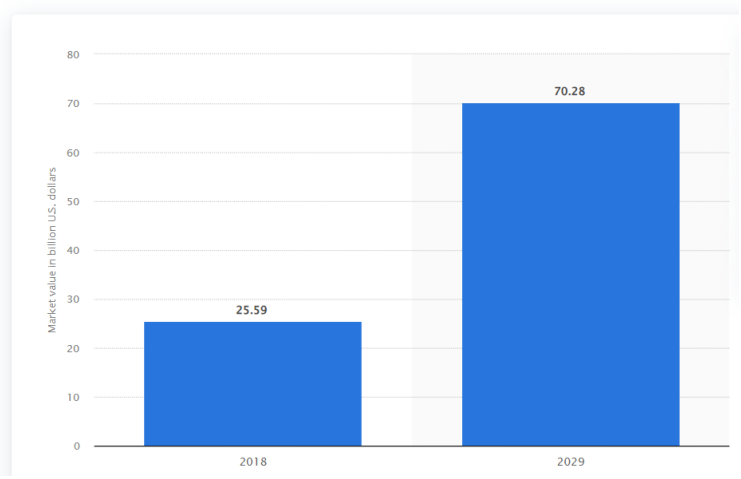

Figure 1 – Global UAV Market Value in 2018 and 2029 in Billion USD

As UAV technology continues to evolve and its applications expand, various drone models have emerged to cater to specific needs. Among these, the quadcopter has become the most widely used UAV configuration due to its stability, ease of control, and versatility in both commercial and recreational applications (Drone Pilot Ground School, n.d.) [3].

Beyond commercial and industrial applications, UAVs play an essential role in healthcare and emergency response. They have proven highly effective in medical supply transportation, especially in critical situations where rapid delivery is necessary. During the COVID-19 pandemic, UAVs were widely deployed for various healthcare tasks, as presented in Figure 2.

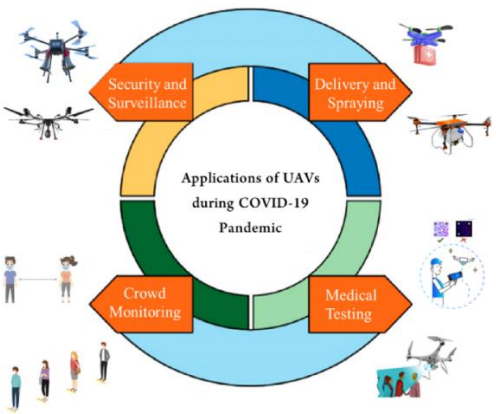

Figure 2: Applications of UAV during Pandemic

In 2020, UAVs were utilised for COVID-19 response efforts across the USA, China, Chile, and other countries. Notably, Zipline, in collaboration with Novant Health, successfully used UAVs to deliver vaccines in North Carolina, USA, showcasing their efficiency in healthcare logistics. These developments further highlight the potential of UAVs in public health and emergency response, emphasising the importance of optimising their performance for hovering, endurance, and payload-carrying capabilities [1].

The challenge: Hovering Efficiency of Propeller in Quadcopters

Despite their effectiveness in such missions, the performance of UAVs is directly influenced by their aerodynamic efficiency. In particular, the efficiency of quadcopter propellers plays a vital role in determining flight stability, energy consumption, and thrust generation. Propeller geometry, including blade shape, airfoil selection, pitch distribution, and tip design, significantly impacts how efficiently a drone can generate lift while minimising energy losses (ResearchGate, 2024) [4]. Therefore, optimising propeller design is crucial for enhancing hovering capability, endurance, and payload capacity, particularly in mission-critical applications such as medical supply transport and emergency response.

Standard commercial propellers, such as APC propellers, are widely used in UAV applications but are often designed for general-purpose performance rather than optimised for specific flight modes. These propellers face several limitations:

- Inefficient hover performance – Many commercial propellers are optimised for high-speed forward flight but lack efficiency in hovering and endurance-focused missions.

- High power consumption – Poorly optimised propeller geometries result in increased drag and unnecessary power usage, thereby reducing flight time.

- Aerodynamic interference – In quadcopters, the proximity of multiple propellers can create airflow disturbances, leading to turbulence and reduced thrust efficiency (Aviation Stack Exchange, n.d.) [5].

Research has demonstrated that modifying propeller geometry—particularly pitch distribution, chord length, and tip design—can significantly enhance thrust efficiency while reducing energy loss (S. A. H. Mohsan et al., 2023) [1]. Additionally, material flexibility can affect aerodynamic efficiency, as propeller blades experience deformation at high rotational speeds, leading to reduced thrust and increased power consumption (Journals SAGE, 2023) [6].

1.1 PROJECT MOTIVATION

Given these challenges, this project aims to optimise the aerodynamic efficiency of a rotating quadcopter propeller by focusing on hovering. Unlike standard APC propellers, which are often compromised for versatility, this research explores optimised blade geometry that enhances hover efficiency by refining propeller geometry.

1.2 PROJECT OBJECTIVE

The objective of this project is to conduct a comprehensive Computational Fluid Dynamics (CFD) analysis of an APC propeller using the Moving Reference Frame (MRF) approach. This study aims to evaluate the aerodynamic performance of the propeller by analysing key parameters such as thrust coefficient, power coefficient, pressure distribution, and wake flow characteristics. The CFD results will be validated against experimental data to ensure accuracy, and a mesh independence study will be conducted to determine the optimal mesh resolution for precise and computationally efficient simulations.

Based on the findings from literature review, the propeller will be redesigned to enhance aerodynamic efficiency, considering factors such as blade geometry modifications. A second round of CFD simulations will be conducted on the redesigned propeller, using the refined mesh settings, to assess improvements in performance metrics. The impact of design modifications on thrust, torque, and power efficiency will be evaluated to determine the effectiveness of the new configuration.

To ensure the accuracy and reliability of the numerical model, CFD simulation results will be validated against wind tunnel data from other research database. Additionally, the study will explore how operating conditions such as rotational speed and flow characteristics influence the propeller's aerodynamic behaviour.

By integrating CFD simulation, design optimisation, and performance validation, this research aims to contribute to the development of more efficient UAV propulsion systems. The ultimate goal is to enhance the aerodynamic efficiency of the propeller, leading to improved drone hovering performance, reduced power consumption, and extended flight endurance.

1.3 LITERATURE REVIEW

The study of propeller aerodynamics is essential for understanding the forces and flow characteristics that govern propeller performance. Over the years, researchers have utilised both experimental and computational methods to analyse and optimise propeller designs. This section reviews fundamental aerodynamic principles, key performance parameters, experimental and numerical approaches, and optimisation studies related to propellers.

1.3.1 Overview of Propeller Aerodynamics

A propeller converts rotational energy into thrust. It consists of blades that rotate around a central hub, creating a pressure difference between the forward and rear surfaces, thereby generating thrust [7]. Figure 3 illustrates the working principle of a propeller [8].

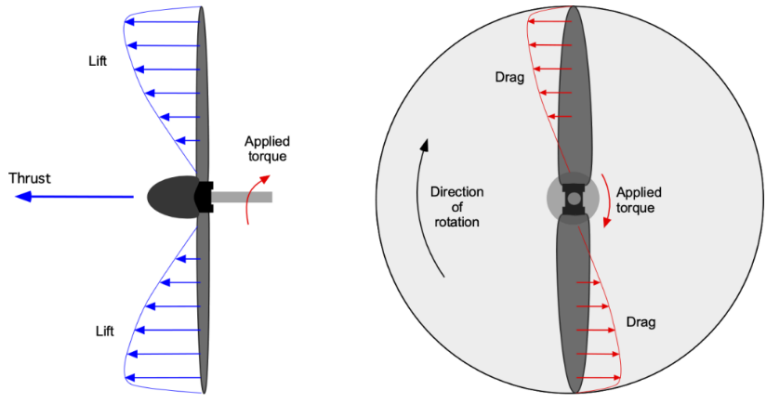

The propeller's rotating blades are each designed to produce a lift force, so the propeller has a net thrust. A torque (and so power) is needed to do this, delivered through the propeller shaft.

Figure 3: Working principle of a Propeller

Propeller blades are twisted along their span to maintain an optimal angle of attack across their length, improving efficiency and thrust generation. Each blade functions as an airfoil, with the pitch angle highest at the root and gradually decreasing toward the tip. This variation, known as wash-out, ensures that each section operates near its most aerodynamically efficient condition. The total twist can reach 40 degrees, significantly more than on aircraft wings, optimising thrust while minimising drag [8]. Figure 4 illustrates the propeller blade twist, which optimises the angle of attack along the span for maximum aerodynamic efficiency.

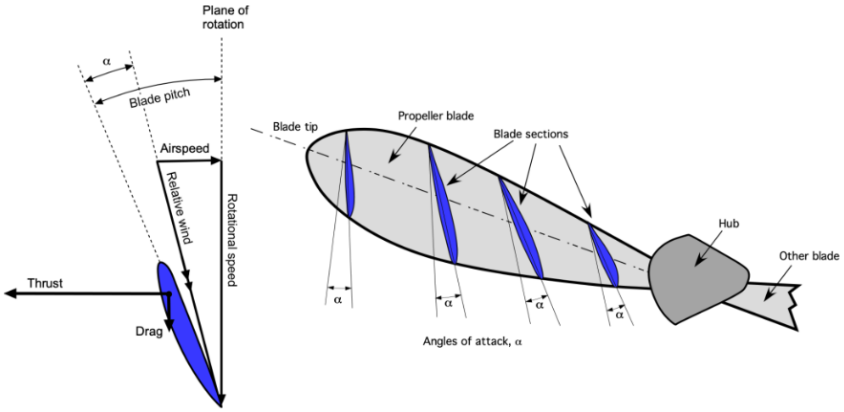

A propeller blade is inevitably twisted along its length, the twist being used to optimize the angles of attack for the best aerodynamic efficiency.

Figure 4: Propeller Blade Twist Angle

1.3.2 Propeller Theory

1.3.2.1 Momentum Theory

The Rankine-Froude propeller theory models a propeller as an ideal actuator disk that increases the momentum and kinetic energy of the air passing through it, shown in Figure 5. This theory explains how a propeller generates thrust by applying a force to the air, creating a pressure difference across the disk. The resulting thrust is directed upstream, while the airflow is accelerated downstream, illustrating the fundamental principle of momentum transfer in propeller operation. [8]

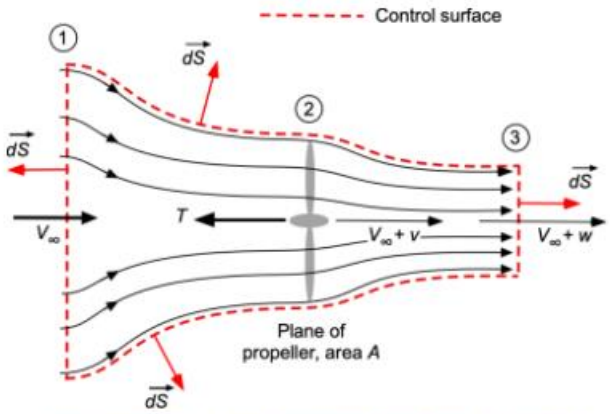

Control volume used for the momentum theory analysis of a single thrusting propeller.

Figure 5: Momentum Theory of Propeller

From Figure 5, the propeller is analysed using a control volume that includes the upstream (1), propeller plane (2), and downstream (3) regions. Initially, the free-stream velocity, V_∞ is uniform before reaching the propeller. As the flow approaches the propeller, it is slightly accelerated due to the suction effect, increasing to $V_\infty + v$. At the propeller plane, the airflow experiences a pressure rise as thrust is applied, imparting momentum to the flow. Downstream, the velocity further increases to $V_\infty + v + w$, where w represents the total acceleration induced by the propeller. Eventually, in the far wake, the static pressure recovers to ambient conditions P_∞. This model assumes steady, one-dimensional, incompressible flow and neglects rotational effects, providing a simplified yet effective means of estimating propeller thrust based on velocity and momentum changes.

The propeller's performance is evaluated based on the principles of conservation laws.

Conservation of Mass

The mass flow rate ($\dot{m}$) must remain constant as air moves through the control volume. Since the propeller has a known disc area (A), the mass flow rate equation is given by:

$$\dot{m} = P_\infty A\,(V_\infty + v) \tag{1}$$

Where

$$A = \frac{\pi d^2}{4} \tag{2}$$

Conservation of Momentum

The net force applied by the propeller to the fluid must equal the change in momentum. The force exerted by the fluid is determined by:

$$F_{fluid} = -\dot{m}V_\infty + \dot{m}(V_\infty + w) \tag{3}$$

Therefore, since Thrust (T) applied by the propeller must equal the net force imparted to the fluid due to the change in momentum across the control volume, it can be expressed as:

$$T = \dot{m}w \tag{4}$$

Conservation of Energy

The work done by the propeller on the air must be equal to the increase in kinetic energy of the slipstream. The total power input to the airflow is:

$$\dot{T}(V_\infty + v) = \frac{1}{2}\dot{m}(V_\infty + w)^2 \tag{5}$$

Hence, the power required for thrust generation is given by:

$$P \doteq T(V_\infty + v) = \frac{1}{2}\dot{m}(2V_\infty w + w^2) \tag{6}$$

Momentum theory helps establish the relationship between thrust and airflow velocity changes, which in turn affects thrust coefficient, C_T which is a non-dimensional parameter used to compare propeller efficiency across different conditions A higher velocity increment (w) leads to a higher thrust coefficient, but excessive values can reduce efficiency.

$$C_T = \frac{T}{\rho n^2 D^4} \tag{7}$$

Similarly, the torque coefficient, C_Q is given by:

$$C_Q = \frac{Q}{\rho n^2 D^5} \tag{8}$$

The power coefficient, C_P is co-related to the torque coefficient, given by:

$$C_P = C_Q \cdot 2\pi \tag{9}$$

1.3.2.2 Blade Element Theory

Blade Element Theory (BET) is a method used to predict propeller performance by dividing the blade into multiple independent sections along its length, shown in Figure 6. At each section, a force balance is applied considering two-dimensional lift and drag forces, along with the thrust and torque produced. Simultaneously, a balance of axial and angular momentum is maintained. This approach results in a set of non-linear equations that can be solved iteratively for each blade section, allowing for the summation of sectional thrust and torque to predict the overall propeller performance [9].

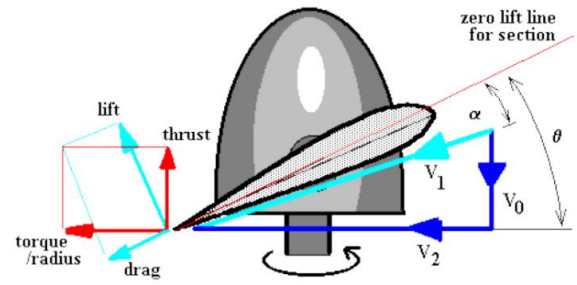

Figure 6: Basis of Blade Element Theory

Referring to Figure 6, the propeller blade is set at a fixed geometric pitch angle (θ), and the incoming flow creates a local angle of attack at each blade section. The lift and drag forces on the section are determined using 2D aerofoil properties, referencing the zero-lift line instead of the chord line. These forces are then resolved into components normal (thrust) and parallel (torque) to the propeller disc, allowing the total thrust and torque of the propeller to be determined by summing contributions from all blade elements.

From the blade elements, the flow angle is defined as the difference between the pitch angle and angle of attack (AoA).

$$\varphi = \theta - \alpha \tag{10}$$

Lift force (ΔL) and drag force (ΔD) for the blade element are derived from airfoil lift and drag coefficients (C_L and C_D):

$$\Delta L = C_L \frac{1}{2} \rho V^2 c \, dr \tag{11}$$

$$\Delta D = C_D \frac{1}{2} \rho V^2 c \, dr \tag{12}$$

Since each small blade section generates lift (ΔL) and drag (ΔD), their contributions to thrust and torque are resolved as follows:

- Thrust: The component of lift that contributes to thrust minus the drag component acting against it:

$$\Delta T = \Delta L \cos(\varphi) - \Delta D \sin(\varphi) \tag{13}$$

- Torque: The moment around the propeller axis, which includes the effect of drag and lift components acting tangentially.

$$\frac{\Delta Q}{r} = \Delta D \cos(\varphi) + \Delta L \sin(\varphi) \tag{14}$$

If the propeller has B blades, the contributions from each blade element are summed across all blades to obtain the total thrust and torque:

Thrust per blade element (generated by lift component while drag acts against it):

$$\Delta T = \frac{1}{2} \rho V^2 c (C_L \cos(\varphi) - C_D \sin(\varphi)) \, B \, dr \tag{15}$$

Torque per blade element (influenced by both drag and lift):

$$\Delta Q = \frac{1}{2} \rho V^2 c (C_D \cos(\varphi) - C_L \sin(\varphi)) \, B \, r \, dr \tag{16}$$

1.3.3 Propeller Performance Parameters

The efficiency of a propeller is determined by its chord line, pitch, blade angle, and angle of attack. These factors work together to optimise thrust, minimise drag, and improve aerodynamic performance. Proper blade twist and pitch distribution ensure efficient airflow management, making propeller design critical for UAV performance, endurance, and fuel efficiency [10]. Figure 7 illustrates the factors influencing the propeller efficiency [11].

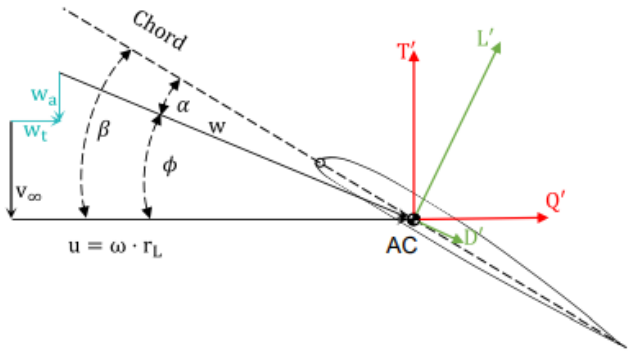

Figure 7: Factors Influencing Propeller Efficiency

Chord Line

The chord line is an imaginary reference extending from the leading to the trailing edge of the blade. It helps define the blade angle, pitch, and aerodynamic shape, affecting thrust and efficiency.

Pitch

Pitch refers to the theoretical distance a propeller would move forward in one revolution if there were no slippage. It functions similarly to a screw, where a higher pitch means the propeller moves more air per rotation, increasing forward thrust but requiring more power [11].

The pitch is not constant along the blade—it varies from hub to tip:

- Steeper near the hub to account for lower rotational speed.
- Shallower towards the tip where rotational velocity is higher.

Pitch can be calculated with the equation:

$$Pitch = 2.36 \times \frac{D \times H}{W} \tag{17}$$

The variation in pitch ensures that the angle of attack remains more uniform across the blade, improving overall efficiency.

Blade Angle

The blade angle is the angle between the chord line and the plane of rotation of the propeller. It determines how much air the blade displaces and is typically measured at a specific point along the blade's length.

While blade angle and pitch are related, they are not the same:

- Blade angle is a geometric property of the blade.

- Pitch determines how much air is moved per rotation and is influenced by the blade angle.

A higher blade angle generally results in a higher pitch, increasing forward thrust but also increasing drag and power demand.

Angle of Attack (AoA)

The angle of attack is the angle between the oncoming airflow and the chord line of the propeller blade. It directly influences the lift and drag forces generated by the blade:

- Increasing the AoA results in more lift and induced drag.
- At a critical AoA, the blade stalls, reducing thrust efficiency.

To maintain optimal AoA along the blade, propellers have a twist—steeper near the hub and shallower at the tip—to compensate for varying rotational speeds along the blade. This helps to:

- Prevent stall at the root where speed is lower.
- Reduce unnecessary drag at the tip where speed is higher.

1.3.4 Propeller Geometry Optimisation

While various parameters such as pitch, diameter, and blade count significantly influence a propeller's aerodynamic performance, these specifications are typically standardised and readily available in commercially manufactured propellers—such as those from the APC series, which offer a wide range of pitch and diameter options. Therefore, although these parameters are critical, the focus of this report is specifically on evaluating the influence of geometric features, such as swept-back tips and downward winglets, as they offer potential performance improvements without altering the fundamental sizing of the propeller. In which, the propeller geometry optimisation will be discussed in this section of the report.

1.3.4.1 Swept Blade

The introduction of swept blades in propeller design has been widely studied as a method to enhance aerodynamic performance, reduce noise, and improve efficiency at higher advance ratios. Unlike unswept blades, where the chord line remains aligned with the rotational plane, swept blades feature a backward or forward inclination that alters the aerodynamic loading distribution across the blade span [12]. Figure 8 illustrates the difference between swept and unswept propeller blade.

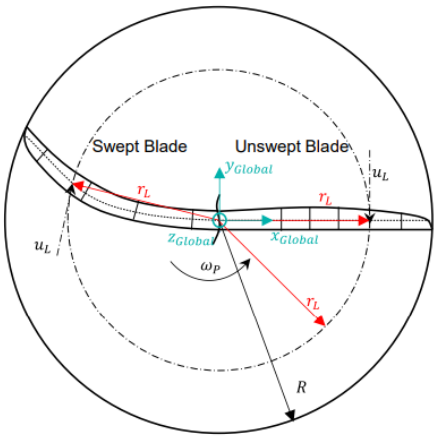

Figure 8: Difference between Swept and Unswept Blade

Blade sweep influences several key aerodynamic properties, including:

- Thrust Generation
  Backward-swept blades tend to generate more thrust at high advance ratios (J) due to reduced compressibility effects and improved wake characteristics (Bergmann et al., 2021).

- Efficiency
  While swept blades improve performance in specific flight conditions, they may introduce additional drag components, affecting overall propulsive efficiency.

- Load Distribution
  The redistribution of aerodynamic loads along the blade span leads to changes in lift and drag characteristics, impacting the structural and dynamic response of the propeller.

Propeller sweep can be classified into two types: forward sweep and backward sweep. Table 1 outlines the key differences between these sweep types along with their respective characteristics.

Forward Sweep	Backward Sweep
• Reduces the onset of compressibility effects at the blade tip. • Improves efficiency at higher rotational speeds. • Increases operational range by maintaining thrust at higher advance ratios. • Commonly used in high-speed UAVs and aircraft propulsion.	• Can enhance static thrust performance. • Used in low-speed applications where initial acceleration is critical. • May result in reduced efficiency at higher velocities due to increased flow separation.

Table 1: Characteristics of Forward and Backward Sweep

1.3.4.2 Angle of Attack

The AoA affects the performance of propeller blades. According to a study conducted by Basset, A., & Cadoux, F. (2019), as the propeller thrust, and power coefficient increases with

the disk angles. Notably, at a disk angle of 90°, the propellers function similarly to rotary wings, generating lift and drag forces instead of traditional thrust and torque [13]. This highlights the significant impact of disk angle-of-attack on propeller performance, offering valuable insights for the design and operation of small UAVs that may experience varied flight attitudes.

1.3.4.3 Downward Winglets

Downward Winglets are aerodynamic modifications applied to the tips of propeller blades to improve efficiency and reduce energy losses. Unlike upward winglets, which are commonly seen on aircraft wings, downward winglets are designed to control vortex formation, minimise drag, and enhance thrust production in specific flight conditions. [14]

The implementation of downward winglets offers the following advantages:

- Reduction of Tip Vortex Strength
  At the blade tip, high-pressure air from the lower surface spills over to the low-pressure region above, forming tip vortices. These vortices cause induced drag, which reduces propeller efficiency. Downward winglets redirect the vortex flow downward and away from the propeller disc, weakening the vortex strength and reducing energy loss, as shown in Figure 9.

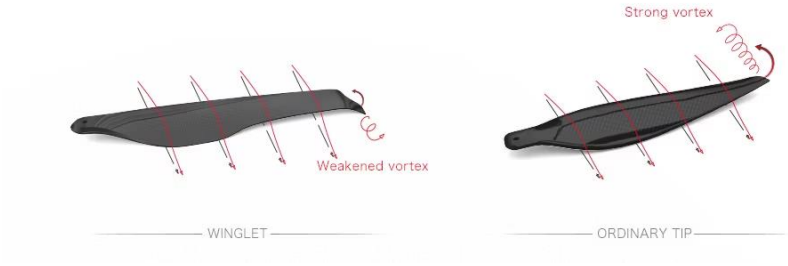

Figure 9: Effect of Wingtip Vortices on Downward Winglets

- Improved Lift Distribution Across the Blade
  A standard propeller blade experiences non-uniform lift distribution, with high loading at the tip causing inefficiencies. Implementing downward wingtip alters the local flow dynamics, spreading the lift distribution more evenly along the blade span. This results in a higher effective lift-to-drag ratio, improving aerodynamic performance.

- Reduction of Induced Drag
  Induced drag arises from airflow circulation around the blade tip, exacerbated by strong vortices. By reorienting the tip vortex downward, a downward wingtip reduces the component of drag acting against the blade's forward motion. This allows the propeller to generate more thrust with the same power input.

- Enhanced Propeller Efficiency at High Advance Ratios
  At high advance ratios (J), where the forward velocity of the aircraft is significant relative to the rotational speed, propeller blades experience flow separation at the tip. Downward wingtips delay flow separation by controlling the local flow pattern, ensuring smoother airflow over the tip region. This maintains higher efficiency at high-speed conditions, where traditional tips would lose performance.

- Noise Reduction and Energy Conservation

Turbulent vortices at the tip are a major source of noise in propeller-driven aircraft and UAVs. Downward wingtips alter the vortex structure, reducing turbulence without compromising thrust. Less turbulent energy means less wasted power, improving the overall efficiency of the propulsion system.

1.3.5 Wind Tunnel and CFD Experiments on Propeller

CFD is a crucial tool for analysing propeller aerodynamics, particularly in UAV applications, allowing for the prediction of flow behaviour, thrust, and efficiency without extensive physical testing. Among CFD techniques, the MRF approach is widely used, as it models propeller rotation in a steady-state reference frame, reducing computational cost while maintaining accuracy. Unlike transient simulations, MRF simplifies calculations, making it a practical choice for aerodynamic analysis.

Despite CFD's capabilities, wind tunnel experiments remain essential for validation, providing direct measurements of thrust, torque, and efficiency. Comparative studies, such as those by Basset and Cadoux (2019) [15], verify strong correlations between CFD and experimental data, particularly in thrust and power coefficient trends. Similarly, Ahmed and Rajendran (2017) [16] validated the MRF approach for an APC propeller at 3008 RPM, demonstrating a close match between numerical and experimental results (shown in Figure 10), reinforcing CFD's reliability in propeller analysis.

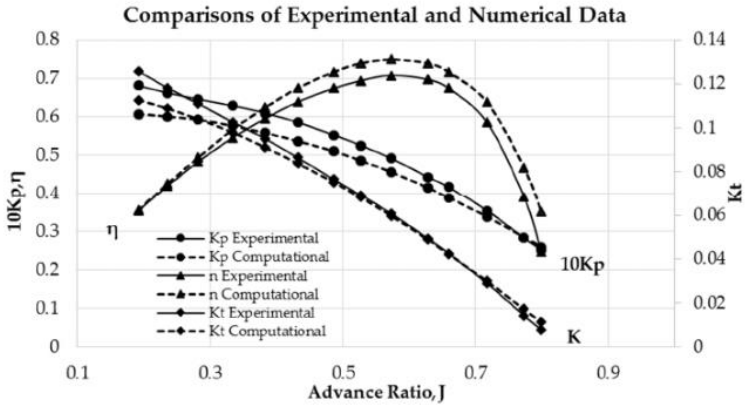

Figure 10: CFD Validation by Ahmed and Rajendran

This study establishes a robust foundation for CFD-based propeller analysis, demonstrating the suitability and reliability of the MRF method for modelling small-scale propeller performance. By combining experimental validation with numerical simulations, it ensures a comprehensive understanding of aerodynamic behaviour.

While both CFD and wind tunnel testing offer valuable insights into propeller performance, each method comes with its own set of advantages and limitations.

Strengths of CFD in Propeller Studies

- Geometry-based Performance Evaluation:
  CFD allows engineers to simulate airflow around the propeller blades, providing detailed insight into how geometry affects thrust, drag, and power consumption [17].

- Rapid Testing of Design Variants:
  It enables quick assessment of design changes—such as modifications in blade shape, pitch, and number of blades—without the need for physical prototypes [18].

- Identification of Problem Areas:
  CFD helps detect regions with high drag, flow separation, or cavitation, guiding designers to make targeted improvements [17]. For instance, one study found that tilting a propeller shaft by just 8 degrees reduced its interaction with the hull, resulting in a 20% increase in effective thrust [19].

- Cost and Time Efficiency:
  Unlike traditional wind tunnel or physical testing, CFD supports fast and iterative refinement at a much lower cost, making it ideal for early-stage design exploration.

Limitations of CFD in Propeller Studies

- Limited Accuracy for Transient Effects:
  Steady-state methods like MRF cannot capture unsteady phenomena such as vortex shedding, dynamic stall, and wake-blade interactions, which are critical for accurate power prediction.

- Validation Requirement:
  CFD results require experimental validation to confirm their reliability, especially for new designs or operating conditions.

- Computational Resources:
  High-resolution simulations (e.g., LES or transient models) demand significant computational power and time.

1.3.6 Importance of Turbulence Modelling in Propeller CFD

The accuracy of CFD simulations depends on factors such as turbulence modelling, mesh quality, and solver selection. Studies indicate that the k-ω SST turbulence model provides precise predictions of boundary layer behaviour and tip vortex structures, making it a preferred choice for propeller aerodynamics (Menter, 1994) [20]. Additionally, grid refinement studies play a crucial role in maintaining numerical stability, where finer meshes improve wake resolution but increase computational cost. To balance accuracy and efficiency, hybrid approaches like BET-CFD coupling integrate Blade Element Theory (BET) corrections with RANS simulations, reducing computational load while maintaining aerodynamic fidelity (Brandt & Selig, 2011) [21].

According to Wang and Walters (2012) [22], the accuracy of CFD simulations in predicting propeller performance depends heavily on the choice of turbulence model. These models approximate turbulent flow behaviour, helping to capture complex aerodynamic effects.

Some of the common turbulence model include:

- K-Epsilon ($k - \varepsilon$) model:

The $k-\varepsilon$ model is widely used but struggles with adverse pressure gradients and flow separation.

- K-Omaga ($k-\omega$) model:
  The $k-\omega$ model offers better near-wall accuracy but is sensitive to free-stream conditions.

- Shear Stress Transport (SST) Model:
  The SST model is a hybrid of k-ω and k-ε, improving predictions in separated flows.

The k-ω SST model was selected for this experimental study. It is widely favoured for propeller CFD analysis due to its robust near-wall resolution and ability to handle flow separation and strong pressure gradients. Its adaptability makes it well-suited for simulating both boundary layer and free-stream turbulence [16].

2 METHODOLOGY

2.1 CFD FRAMEWORK

The CFD framework used in this project is designed to evaluate and optimise the aerodynamic performance of a quadcopter propeller under static hovering conditions, using the MRF approach. This method provides a reliable alternative to wind tunnel testing by simulating the airflow around the rotating propeller and analysing key performance metrics such as thrust coefficient, power coefficient, pressure distribution, and wake behaviour.

Domain Setup

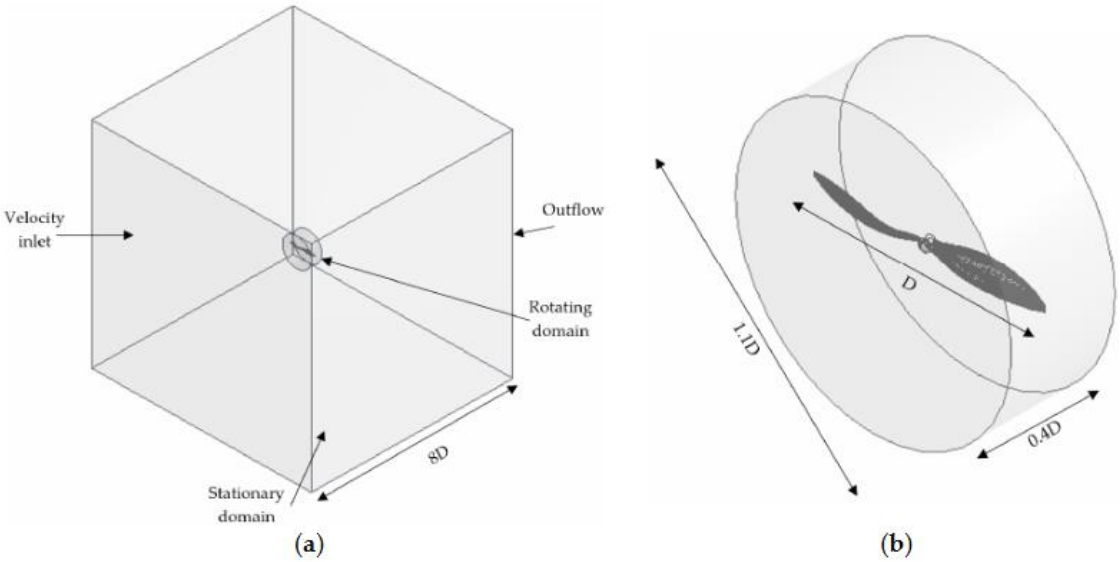

Figure 11: (a) Stationary domain and boundary conditions. The boundary conditions include an inlet, outlet, stationary domain, and rotating domain;(b) Rotating domain

The first step in the simulation process involves geometry preparation and domain setup. The APC propeller Computer Aided Design (CAD) model is imported into the CFD environment, ensuring it is correctly scaled and positioned. The computational domain is divided into two distinct regions: a rotating zone encompassing the propeller and a stationary zone representing the surrounding airflow. The optimal domain size is shown in Figure 11, based on the setup used in the study by Ahmed, H. and Rajendran, P. (2017) [16]. To ensure consistency in CFD results and facilitate experimental validation, the same domain parameters were adopted throughout this study. This configuration supports the MRF approach, where the rotating region simulates the propeller's motion while the surrounding stationary region captures external flow interactions.

Meshing

Meshing is a crucial aspect of the simulation process, as it directly influences the accuracy of the results. In this study, face sizing was used exclusively as the meshing control method for the CFD simulation of the propeller using the MRF approach. This decision was based on its simplicity, effectiveness, and ability to provide targeted mesh refinement in critical regions. By applying different face sizing values to specific surfaces—namely the propeller blades, MRF interfaces, MRF rotating volume, and interface and volume walls—the mesh was refined

where it matters most, such as around blade surfaces and at the boundary between rotating and stationary zones. This allowed for accurate resolution of important aerodynamic features including boundary layer development, pressure gradients, and wake interactions, all of which are crucial for predicting thrust and torque under static conditions. Figure 12 shows an illustration of the meshing prior to the mesh independence study.

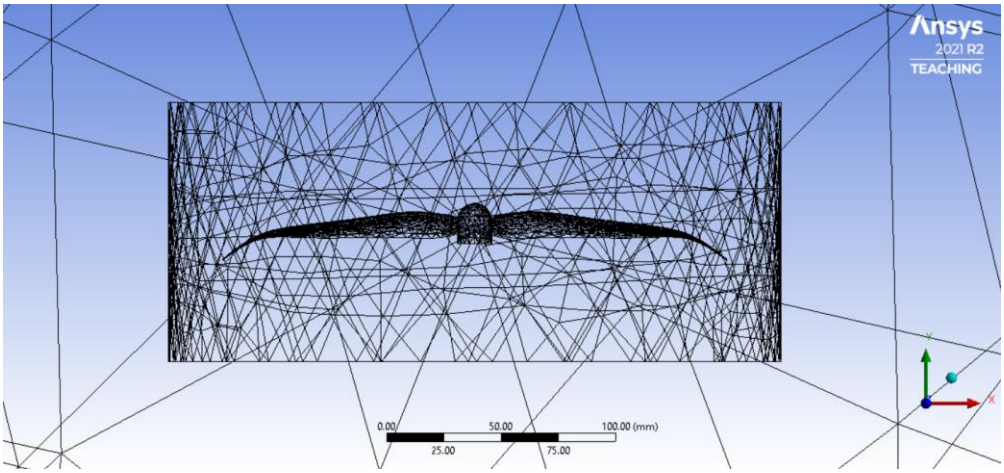

Figure 12: Meshing of Propeller and MRF Region

From Figure 12, it can be observed that graded mesh refinement strategy was applied in this CFD study to balance accuracy and efficiency. The finest mesh was used on the propeller blades to capture detailed aerodynamic features such as pressure gradients and tip vortices, as they are the primary source of thrust. The surrounding MRF region, where significant velocity gradients occur, was assigned a moderate mesh to ensure accurate flow resolution. Lastly, the static region, representing the far-field flow with lower complexity, was meshed coarsely to reduce computational load while preserving overall simulation fidelity.

The MRF method assumes a steady-state rotational reference frame, making surface and interface resolution more critical than complex volume refinement or inflation layers, which are typically used in transient simulations. As such, the use of face sizing alone was sufficient to achieve mesh quality that supports numerical stability and result accuracy, particularly in regions with high velocity gradients. Moreover, this approach ensured mesh consistency across all propeller configurations for the new propeller design, thereby enabling a fair comparison of their aerodynamic performance.

Simulation Setup

Once meshing is completed, the solution setup is initiated. The simulation is performed using the MRF method, with the frame motion approach applied to the rotating domain. This enables the governing equations to be solved within a rotating reference frame, allowing for a steady-state approximation of the propeller's motion without the need for time-dependent simulation. To model turbulence effects accurately, the k-ω SST model was selected. As discussed in section 1.3.6, the model is well-suited for capturing key aerodynamic features such as adverse pressure gradients, flow separation, and vortex shedding, which are commonly observed in propeller flow fields under static conditions. The k-ω SST model offers improved near-wall resolution by leveraging the strengths of the k-ω formulation, while seamlessly transitioning to the k-ε model in the free-stream region for enhanced numerical stability. This hybrid approach ensures a reliable prediction of thrust and torque

Post-Processing

To analyse the propeller's performance, force reports are generated, capturing the thrust and torque distribution acting on the blades. Additionally, contour plots of velocity and pressure are generated to visualise the flow behaviour around the propeller. These results provide insights into aerodynamic efficiency, and potential areas of flow separation, which will be used to refine the propeller design in subsequent iterations.

Mesh Independence Study

A mesh independence study was carried out to determine the optimal mesh resolution for the CFD simulations, ensuring that the results are not significantly influenced by mesh density. The process involved progressive mesh refinement and evaluation of key aerodynamic parameters—particularly thrust—until the solution converged, meaning that further mesh refinement led to negligible changes in the output. By systematically comparing results across varying mesh sizes, the study identified a mesh density that delivered stable and reliable predictions without unnecessary computational cost. This ensures that the final CFD results are independent of mesh resolution, thereby increasing the credibility and accuracy of the simulation outcomes.

Validation

To verify the accuracy of the MRF approach, a validation study was conducted by comparing CFD simulation results with wind tunnel experimental data obtained from UIUC [21]. Two commercially available propellers—APC 10x7" and APC 8x3.8"—were selected for this purpose. Both propellers were simulated under static conditions, and key aerodynamic parameters, thrust and power coefficients were compared against experimental results.

Two different propeller models were tested in the validation process was intended to identify whether the CFD simulations could accurately reproduce consistent performance trends across varying geometries. Observing similar trends in both propellers strengthens confidence in the reliability of the simulation setup and numerical methods. By ensuring that the CFD results align with experimental data for more than one geometry, the accuracy and general applicability of the simulation framework are validated more robustly.

2.2 PROPELLER DESIGN

As the primary objective of this study is to investigate how geometric features influence aerodynamic efficiency, a structured design approach was adopted. A baseline propeller was first developed, serving as a reference model. Based on insights from the literature and initial CFD results, additional aerodynamic features were introduced—such as swept-back tips and downwash winglets—to evaluate their impact on performance.

To ensure fair and consistent comparison, a mesh independence study was first conducted on the baseline propeller to determine the optimal mesh parameters. These same meshing conditions were then applied to all modified propeller designs. This approach ensures that any differences in aerodynamic performance are attributed to the design changes alone, rather than variations in mesh quality or resolution.

Although BET is commonly used in propeller design, it was not adopted in this study due to its known limitations in accurately predicting power—particularly under static or low-speed conditions where unsteady flow effects are dominant. Instead, only Momentum Theory was applied to support the theoretical framework, particularly in computing the thrust and power efficiencies, while CFD simulations provided more detailed and reliable predictions of both thrust and power.

3 VALIDATION

This section shows the validation process of CFD with APC propellers. Validation is a crucial step in any CFD study, as it ensures that the simulation results accurately represent real-world behaviour. In this study, validation is performed by comparing the numerical results with experimental data obtained from the UIUC Propeller Database [21]. This process is essential to establish accuracy of the experimental approach.

3.1 APC 10x7" PROPELLER

The first propeller used for validation is the APC 10x7" propeller[1], shown in Figure 13.

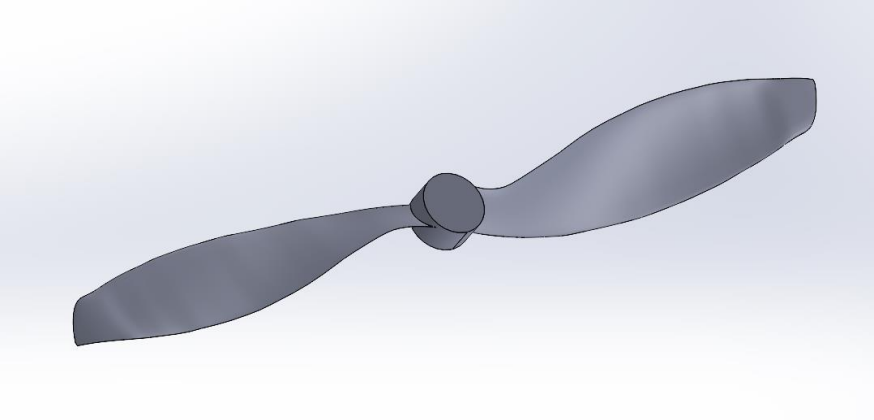

Figure 13: APC 10x7" Propeller used for validation

The APC 10x7" propeller was operated at a rotational speed of 3008 RPM for validation purposes, specifically under static conditions, where both the inlet velocity and advance ratio are negligible. This setup replicates a hovering scenario, in which the propeller generates thrust without any forward motion. Table 2 summarises the data parameters used for validating the APC 10x7" propeller.

Data Parameters for Validation of APC 10x7" Propeller	
Air Density (ρ)	$1.225 kg/m^3$
Rotational Speed (RPM)	$3008 rev/min$
Rotational Speed (ω)	$314.997 rad/sec$
Diameter of Propeller (D)	$0.255 m$
Freestream Velocity	$0 m/s$

Table 2: Data Parameters for Validation of APC 10x7" Propeller

Wind tunnel data from the UIUC [21] Propeller Database indicates that the APC 10x7" propeller exhibits a thrust coefficient of 0.144 and a power coefficient of 0.0686 under static conditions, with the propeller rotating at 3008 RPM and zero inlet velocity. These values serve as benchmark reference points for validating the CFD simulation. Figures 15 and 16 present the wind tunnel experimental graphs showing the variation of thrust and power coefficients for the propeller under static operating conditions.

[1] APC 10x7" propeller CAD model: https://grabcad.com/library/apc-slow-flyer-10-x-7-2

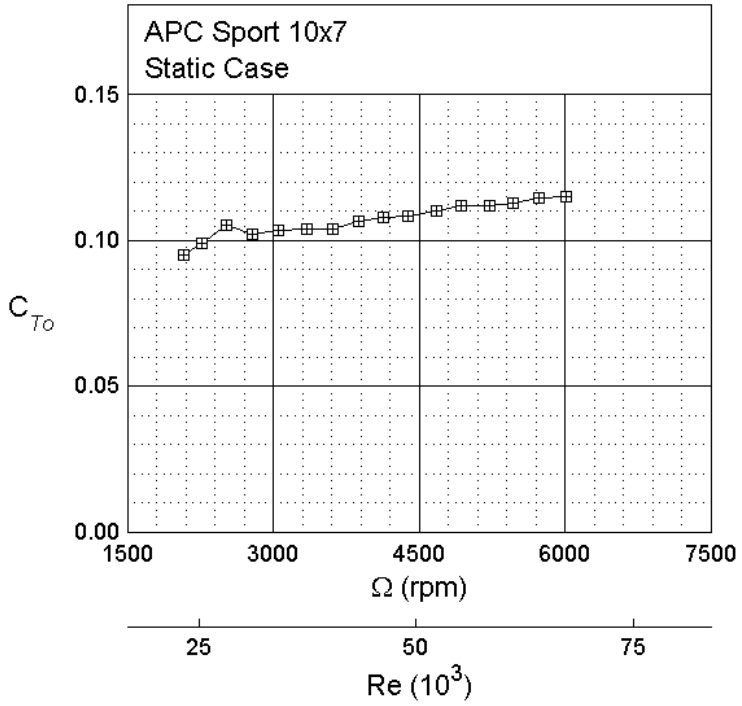

Figure 14: Thrust Coefficient from Wind Tunnel Experiment (APC 10x7")

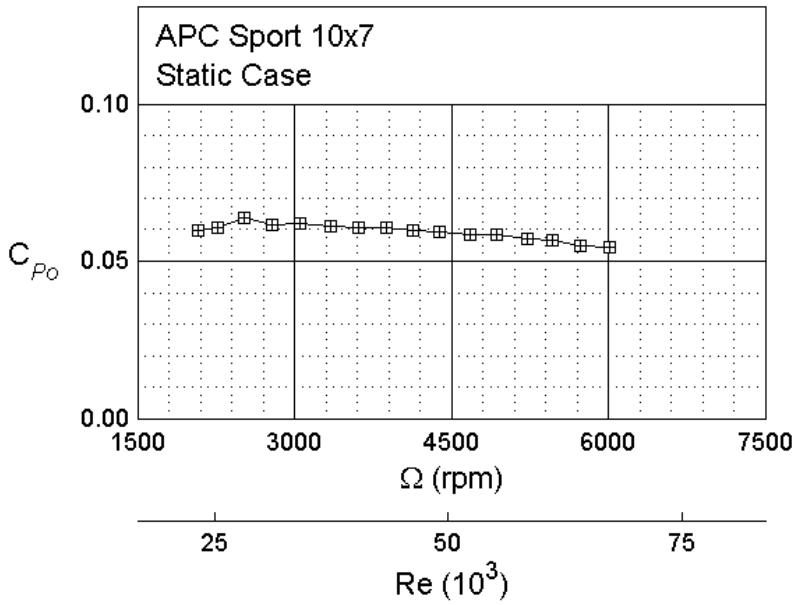

Figure 15: Power coefficient from Wind Tunnel Experiment (APC 10x7")

For mesh independence study, 6 different mesh refinements were tested, ranging from an extra coarse mesh to an extra fine mesh. The grid resolution was progressively increased to assess its impact on thrust and torque.

Table 3 presents the grid resolution details for the APC 10x7" propeller, listing the number of nodes and elements for each mesh refinement level. The different mesh densities assess the impact of grid resolution on simulation accuracy. As the mesh is refined, the number of nodes and elements increases significantly, improving flow resolution at the cost of higher

computational effort. This structured approach ensures that an optimal balance is achieved between accuracy and efficiency during the mesh independence study.

Type of Mesh	No. of Nodes	No. of Elements
Extra Coarse	269654	1430779
Course	425795	2270540
Mid	715011	3830958
Mid Fine	1395630	7495700
Fine	1761371	9404263
Extra Fine	2188836	11692489

Table 3: Grid Resolution for APC 10x7" Propeller

Table 4 presents the thrust and torque values obtained from CFD simulations for respective mesh resolutions.

Type of Mesh	Thrust (N)	Torque (Nm)
Extra Coarse	2.82055	0.06494
Coarse	2.79578	0.06269
Mid	2.71493	0.05993
Mid Fine	2.20260	0.05803
Fine	2.09830	0.05610
Extra Fine	2.04862	0.05505

Table 4: Thrust and Torque Generated by APC 10x7" Propeller

Using the thrust and torque values from Table 4, the thrust and power coefficients were calculated with equations 7, 8, and 9 and compared with wind tunnel experiment data from UIUC [21]. Table 5 presents the calculated coefficients for each mesh resolution alongside the experimental values.

Type of Mesh	CFD Results		UIUC Wind Tunnel Experiment data [21]		Percentage Difference Between CFD and Wind Tunnel Experiments	
	C_T	C_P	C_T	C_P	C_T	C_P
Extra Coarse	0.21667	0.12209	0.144	0.0686	50.48611	77.97376
Coarse	0.21476	0.11866			49.09722	72.97376
Mid	0.20855	0.11343			44.82639	65.34985
Mid Fine	0.16919	0.10983			17.49301	60.10204
Fine	0.16118	0.10618			11.93056	54.78134
Extra Fine	0.15737	0.10419			9.28472	51.88047

Table 5: Comparison of CFD and Wind Tunnel Experiment for Thrust and Power coefficient of APC 10x7" Propeller

From table 5, it can be observed that as the mesh was progressively refined from extra coarse to extra fine, the percentage difference between CFD-predicted and experimental thrust and power coefficients decreased significantly. The results demonstrate a clear convergence trend, with the deviation reducing from over 50% at coarse meshes to less than 10% for the extra fine mesh. Notably, the extra fine mesh achieved a 9.28% difference in thrust coefficient and 51.88% in power coefficient, indicating that thrust predictions are within acceptable accuracy limit of less than 10% deviation.

3.2 APC 8x3.8" PROPELLER

Figure 11 shows the APC 8x3.8" propeller[2], which is used as a secondary test case to further validate the mesh independence study and CFD approach conducted in this study. The same CFD methodology was applied to this propeller to ensure consistency with the APC 10x7" propeller simulations. By analysing a different propeller geometry, this procedure aims to assess the robustness and accuracy of the computational methodology across varying designs and rotational speeds.

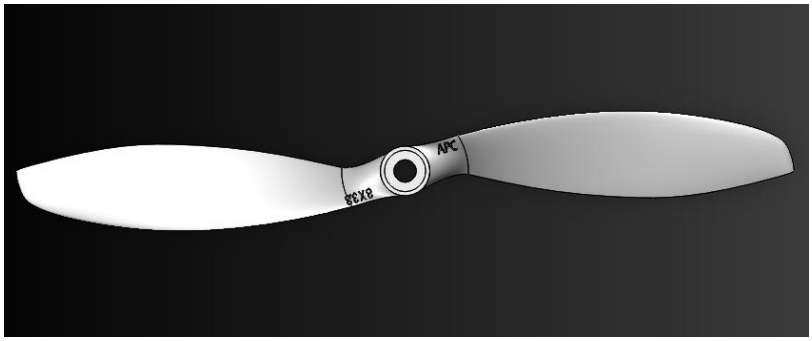

Figure 16: 8x3.8" APC Propeller

The APC 8x3.8" propeller was operated at a rotational speed of 3808 RPM, under static conditions, where both the inlet velocity and advance ratio are negligible. Table 6 summarises the data parameters used for validating the APC 8x3.8" propeller.

Data Parameters for Validation of APC 8x3.8" Propeller	
Air Density (ρ)	$1.225 kg/m^3$
Rotational Speed (RPM)	$3808 rev/min$
Rotational Speed (ω)	$398.773 rad/sec$
Diameter of Propeller (D)	$0.207 m$
Freestream Velocity	$0 m/s$

Table 6: Data Parameters for Validation of APC 8x3.8" Propeller

Wind tunnel data from the UIUC [21] Propeller Database indicates that the APC 8x3.8" propeller exhibits a thrust coefficient of 0.0976 and a power coefficient of 0.0420 under static conditions, with the propeller rotating at 3808 RPM and zero inlet velocity. Figures 15 and 16 present the wind tunnel experimental graphs showing the variation of thrust and power coefficients for the propeller under static operating conditions.

[2] APC 8x3.8" propeller CAD model: https://grabcad.com/library/apc-8-x-3-dot-8-slow-flyer-prop/files

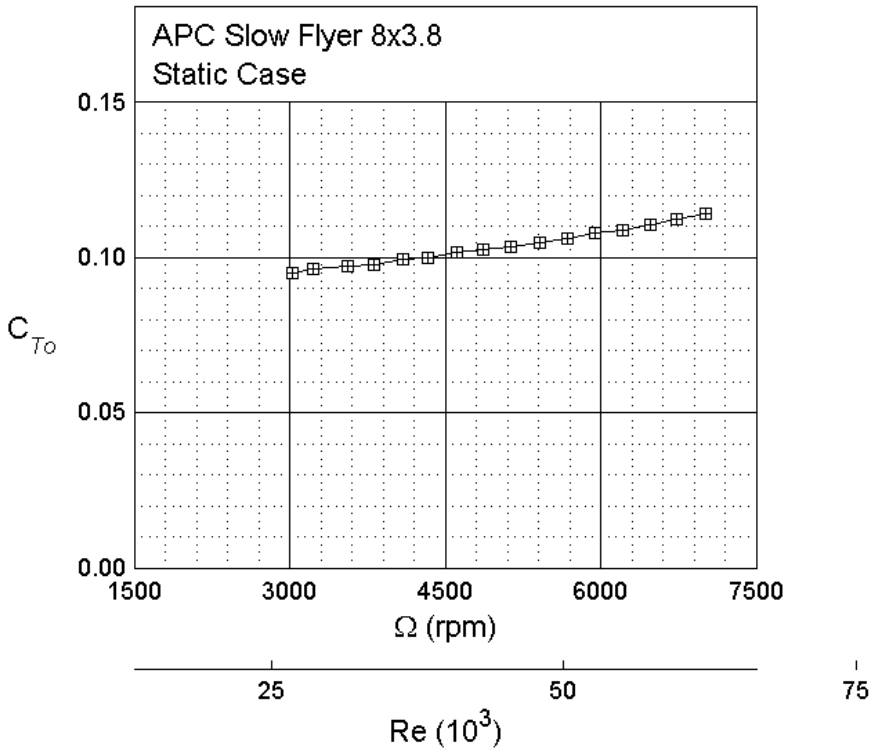

Figure 17: Thrust Coefficient from Wind Tunnel Experiment (APC 8x3.8)

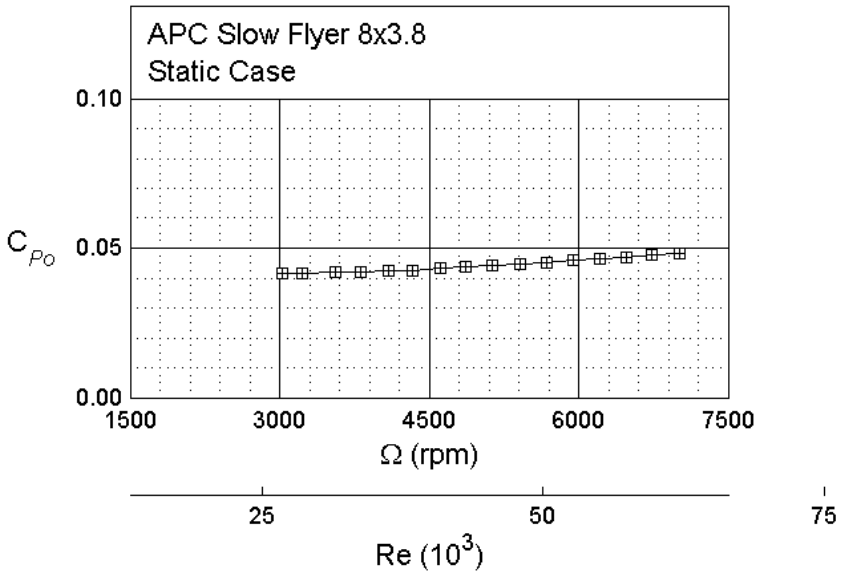

Figure 18: Power coefficient from Wind Tunnel Experiment (APC 8x3.8")

Table 7 presents the grid resolution details for the APC 8x3.8" propeller, listing the number of nodes and elements for each mesh refinement level. Similarly to the APC 10x7" propeller, the APC 8x3.8" propeller also employs six mesh densities, ranging from extra coarse to extra fine.

Type of Mesh	No. of Nodes	No. of Elements
Extra Coarse	134945	726248
Coarse	540725	2902442
Mid	1008838	5427645
Mid Fine	1175825	6321115
Fine	1464928	7878087
Extra Fine	1773301	9541104

Table 7: Grid Resolution for APC 8x3.8" Propeller

Table 8 presents the thrust and torque values obtained from CFD simulations for respective mesh resolutions.

Type of Mesh	Thrust (N)	Torque (Nm)
Extra Coarse	1.34297	0.01991
Coarse	1.16148	0.01812
Mid	1.03336	0.01763
Mid Fine	0.96238	0.01688
Fine	0.96629	0.01715
Extra Fine	0.96450	0.01675

Table 8: Thrust and Torque Generated by APC 8x3.8" Propeller

Using the thrust and torque values from Table 8, the thrust and power coefficients were calculated with equations 7, 8, and 9 and compared with wind tunnel experiment data from UIUC [21]. Table 9 presents the calculated coefficients for each mesh resolution alongside the experimental values.

Type of Mesh	CFD Results		UIUC Wind Tunnel Experiment data [21]		Percentage Difference Between CFD and Wind Tunnel Experiments	
	C_T	C_P	C_T	C_P	C_T	C_P
Extra Coarse	0.14707	0.06606	0.0976	0.0420	50.61475	57.28571
Coarse	0.12719	0.06012			30.31762	43.14286
Mid	0.11316	0.05850			15.94262	39.28571
Mid Fine	0.10539	0.05599			7.89156	33.30952
Fine	0.10582	0.05688			8.45287	35.42857
Extra Fine	0.10562	0.05556			8.21721	32.28571

Table 9: Comparison of CFD and Wind Tunnel Experiment for Thrust and Power coefficient of APC 8x3.8" Propeller

3.3 PROPELLER VALIDATION ANALYSIS

This section presents a detailed analysis of the CFD validation results for both the APC 10x7" and APC 8x3.8" propellers. The trend observed in the mesh independence study helps to validate the accuracy of the CFD simulations by demonstrating the effect of mesh refinement on thrust and power coefficient predictions. The CFD results are further compared against wind tunnel experiments conducted by UIUC [21], ensuring that the numerical methodology aligns with experimental observations.

Both propellers were analysed using the same CFD approach, and a systematic mesh refinement process to assess solution convergence. The percentage deviation between CFD and experimental data highlights the impact of grid resolution on prediction accuracy. Additionally,

the study evaluates how propeller geometry and rotational speed influence aerodynamic performance, reinforcing the reliability of the simulation framework.

3.3.1 Thrust Analysis

Figure 19 shows the thrust comparison between the APC 10x7" and APC 8x3.8" propellers across different mesh resolutions.

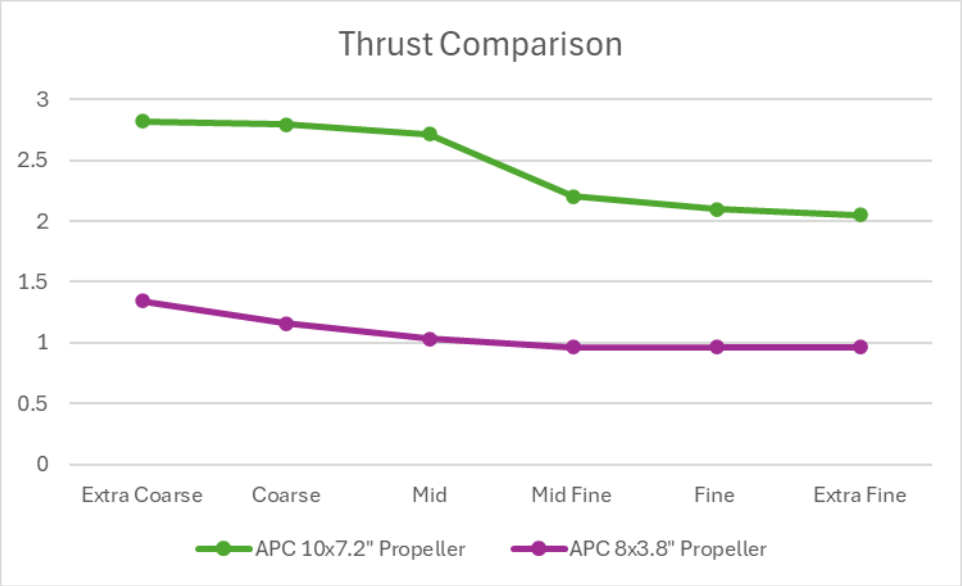

Figure 19: Thrust Comparison

The thrust production trends for both the APC 10x7" and APC 8x3.8" propellers exhibit a similar trend in the mesh independence study, where thrust initially decreases with finer mesh refinement but eventually stabilizes.

For both propellers, the extra coarse and coarse meshes overpredict thrust due to lower grid resolution, which may lead to inaccuracies in capturing boundary layer effects and flow separation. As the mesh is refined, the simulations become more accurate, and the thrust values start to converge. However, beyond a certain level of refinement – mid fine mesh, the thrust remains nearly constant, indicating that further increasing the mesh density does not significantly impact the solution. This stabilisation suggests that numerical errors due to mesh dependency are minimized, ensuring that the CFD results are reliable.

The similarity in convergence behaviour between the two propellers confirms that a well-conducted mesh independence study helps determine the optimal grid resolution for accurate thrust predictions. For the APC 10x7" propeller, the thrust stabilises around the fine mesh resolution, while for the APC 8x3.8" propeller, stability is achieved slightly earlier, around the mid-fine resolution. This observation reinforces that while different propeller designs may require different levels of refinement, they follow the same general trend of convergence toward an accurate solution with diminishing changes in thrust values at finer meshes.

Ultimately, this trend highlights the importance of selecting an optimal mesh resolution to balance computational efficiency and accuracy. These results validate the mesh independence approach used in this study, ensuring that CFD simulations are not overly dependent on mesh density while maintaining a high level of accuracy in thrust predictions.

3.3.2 Torque Analysis

Figure 13 shows the torque comparison between the APC 10x7” and APC 8x3.8” propellers across different mesh resolutions. The results illustrate how torque values decrease as mesh refinement increases, following a trend similar to the thrust analysis.

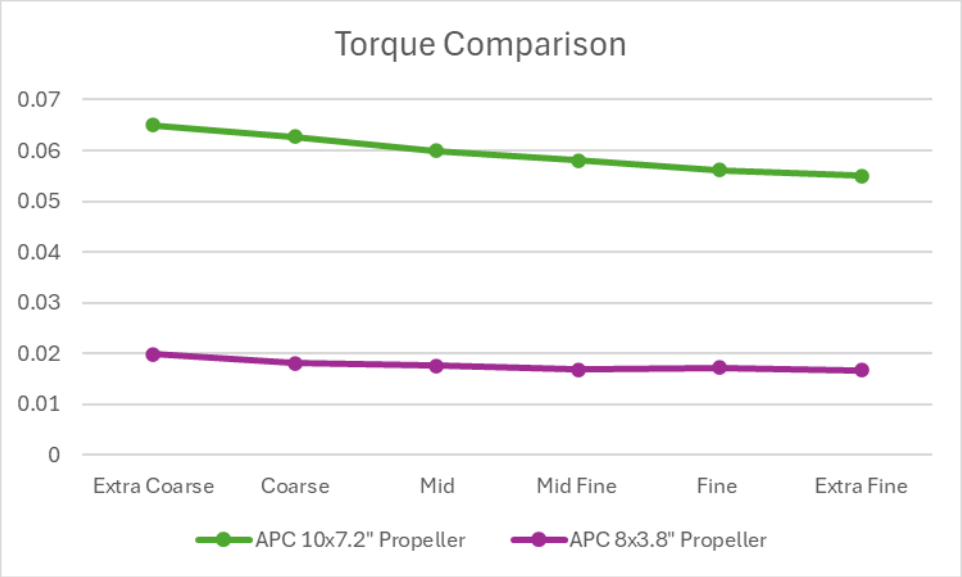

Figure 20: Torque Comparison

For both propellers, the extra coarse and coarse meshes produce slightly higher torque values due to lower grid resolution, which may not fully capture the detailed flow interactions and viscous effects around the blades. As the mesh is refined from mid to extra fine resolution, the torque values gradually stabilise, indicating mesh convergence.

The APC 10x7” propeller exhibits higher torque values compared to the APC 8x3.8” propeller, which is expected due to its larger diameter and pitch, requiring more rotational force to generate thrust. The trend suggests that an optimal mesh resolution for accurate torque prediction is fine mesh for APC 10x7” and mid-fine mesh for APC 8x3.8”, beyond which further refinement offers diminishing returns on accuracy.

3.3.3 Thrust Coefficient Analysis

Figures 21 and 22 illustrate the thrust coefficient variation for the APC 10x7” and APC 8x3.8” propellers across different mesh resolutions, comparing CFD results with wind tunnel experimental data from UIUC [21].

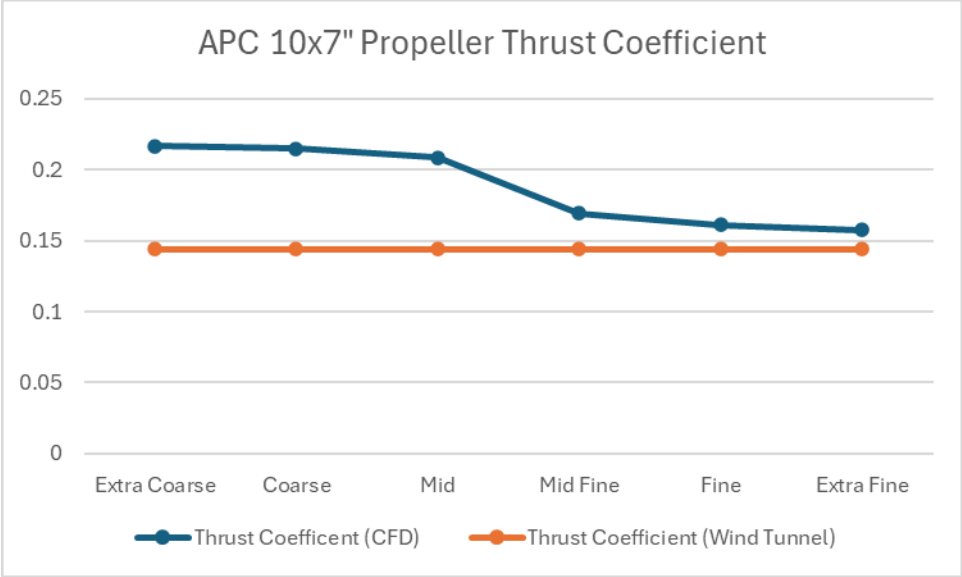

Figure 21: APC 10x7" Propeller Thrust Coefficient Analysis

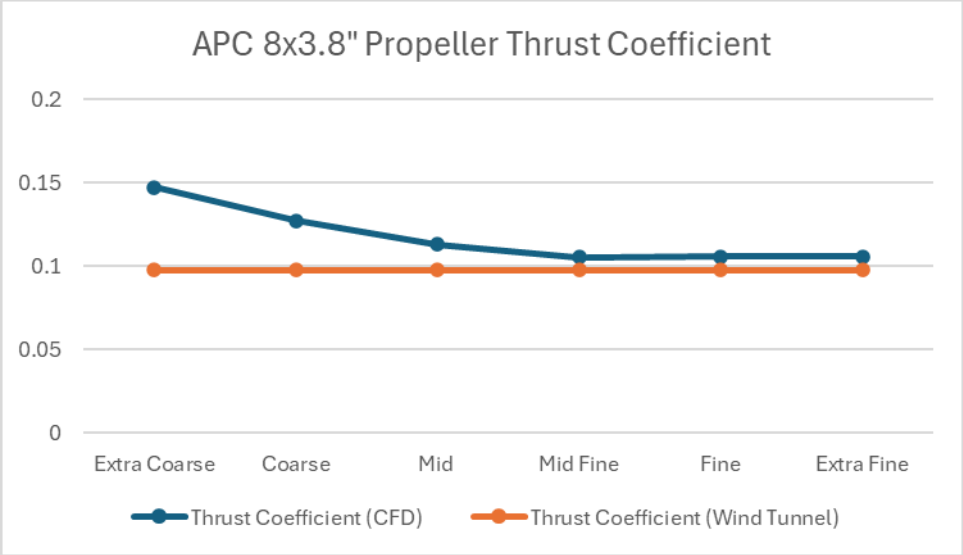

Figure 22: APC 8x3.8" Thrust Coefficient Analysis

For both propellers, the thrust coefficient decreases as the mesh is refined, showing a similar trend observed in the thrust and torque analyses. At coarser mesh levels, CFD predictions overestimate thrust coefficient, likely due to insufficient resolution of near-wall flow and numerical diffusion. As the mesh becomes finer, the thrust coefficient, values align more closely with experimental results, with fine and extra fine meshes showing the best agreement. The APC 10x7" experiences a more noticeable drop between mid and mid-fine, while the APC 8x3.8" converges around mid-fine.

Since the CFD-predicted thrust coefficient closely matches the experimental data, it indicates that the simulation methodology is accurately capturing the aerodynamic forces acting on the propellers. The results suggest that the thrust force is well-resolved using the selected numerical models and boundary conditions, making the simulation framework a dependable tool for propeller performance evaluation.

3.3.4 Power Coefficient Analysis

Figures 23 and 24 illustrate the power coefficient variation for the APC 10x7" and APC 8x3.8" propellers across different mesh resolutions, comparing CFD results with wind tunnel experimental data from UIUC database [21].

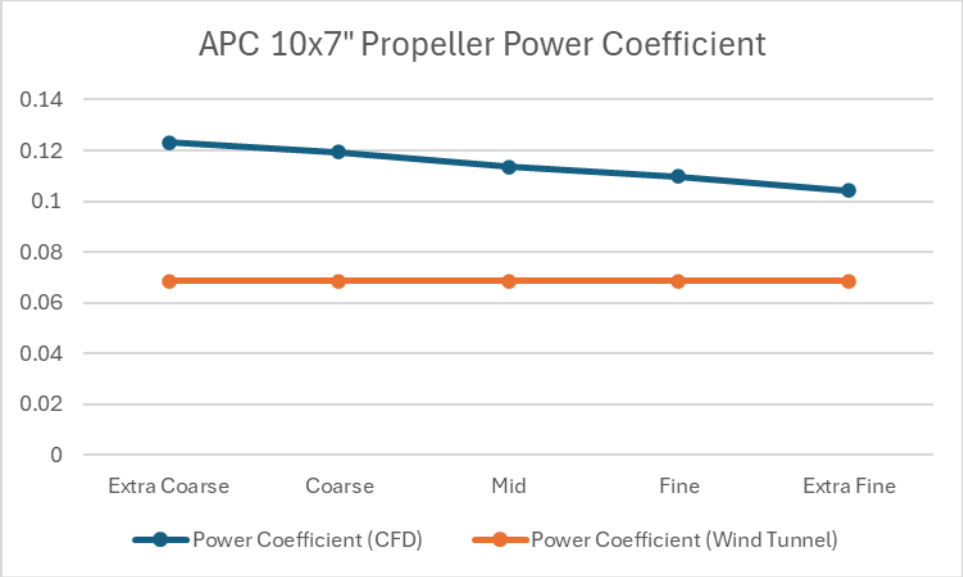

Figure 23: APC 10x7" Power Coefficient Analysis

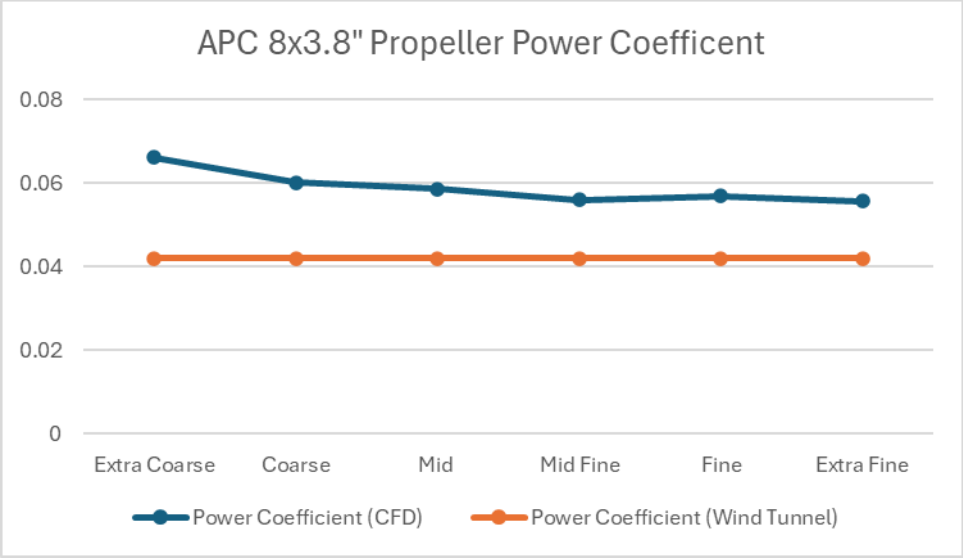

Figure 24: APC 8x3.8" Power Coefficient Analysis

The results indicate that while the power coefficient decreases with mesh refinement, the CFD-predicted values remain consistently higher than the wind tunnel data. This discrepancy is a well-recognised phenomenon in steady-state MRF simulations and has been concluded in various CFD studies. While the thrust coefficient generally aligns well

with experimental data, the power coefficient tends to be overestimated due to inherent limitations of the MRF approach in capturing unsteady aerodynamic effects.

Discrepancies in power coefficient for MRF Simulations

While the MRF approach is effective for predicting steady-state aerodynamic forces such as thrust, it has notable limitations when estimating power coefficient. This is primarily because the MRF method assumes a steady rotational frame and does not resolve time-dependent effects such as blade-wake interactions, unsteady vortex shedding, or dynamic stall. As a result, it may underestimate or overestimate the actual power consumed by the rotating system.

This behaviour is not unique to propeller simulations and has been widely reported across various applications. For example, Rezaeiha et al. (2017) observed that MRF simulations for Darrieus vertical axis wind turbines tend to overpredict power coefficient due to the omission of transient stall effects and azimuthal flow variations [24]. Similarly, Wang et al. (2019) noted in their study of micro turbojet engines that while thrust was accurately captured, the MRF model overestimated shaft power due to the absence of unsteady flow resolution [25]. In stirred-tank reactors, Bakker et al. (2000) found that although mean velocity fields were accurate, power number estimations showed significant deviation from experimental values, further highlighting the limitations of steady-state modelling approaches [26]. Therefore, discrepancies in power coefficient predictions in this study are consistent with known MRF limitations and should be interpreted with caution when evaluating propeller efficiency.

The MRF method assumes a steady-state rotational frame, meaning it does not fully resolve transient blade-wake interactions, dynamic stall, or unsteady vortical structures. As a result, while mean aerodynamic forces such as thrust are captured accurately, power estimations can deviate due to missing transient effects. This behaviour has been commonly observed.

Validation of the CFD Approach

Despite the overprediction observed in the power coefficient, the primary validation metric for this study is the thrust coefficient. Across mesh refinement levels, was shown to stabilise and align closely with experimental wind tunnel data, particularly at finer mesh resolutions. This confirms that the CFD MRF approach reliably captures the steady aerodynamic forces acting on the propeller under static conditions. Given that thrust generation is the dominant performance parameter for assessing propeller efficiency in hovering flight, the CFD predictions can be considered valid and dependable for aerodynamic analysis and optimisation.

4 PROPELLER DESIGN

This section presents the design and aerodynamic evaluation of modified propeller configurations aimed for improving performance under static hovering conditions. Building upon the validated CFD framework, the study begins with a baseline propeller design, which serves as the reference for subsequent comparisons. Based on insights from literature and aerodynamic principles, two enhanced designs were developed—one featuring a swept-back tip, and another incorporating a downward winglet.

The primary objective of these modifications is to improve thrust generation while minimising power consumption, thereby increasing the overall aerodynamic efficiency of the propeller. Each design is systematically analysed and compared against the baseline to assess whether the introduced features contribute to performance improvements.

The performance of the modified propellers is evaluated against the baseline by examining key metrics such as thrust coefficient, power coefficient, and thrust-to-power ratio. This section outlines the rationale for each geometric modification, the implementation process, and the resulting impact on aerodynamic performance.

4.1 BASELINE PROPELLER

A baseline propeller is essential in this study as it serves as a reliable reference for evaluating the effectiveness of geometric modifications. By providing a consistent and validated foundation, the baseline allows for accurate comparison of performance metrics namely, thrust coefficient, power coefficient, and thrust-to-power ratio. It ensures that any observed improvements in the modified designs are directly attributable to the introduced features rather than variations in simulation setup.

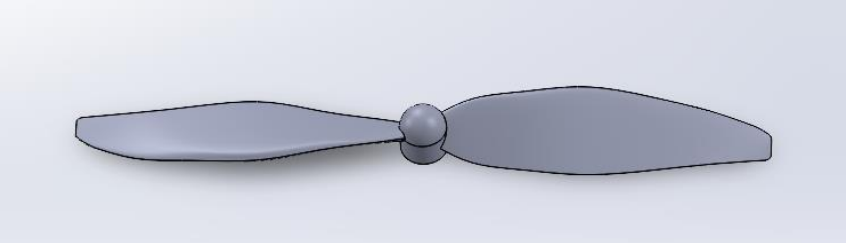

Figure 25: Geometry of Baseline Propeller

A mesh independence study was conducted on the baseline propeller to identify the optimal meshing parameters required for accurate and reliable CFD results. The baseline propeller, like the APC 8x3.8” used in earlier validation, was simulated at a rotational speed of 3808 RPM. The corresponding operating and mesh parameters used in the simulation are summarised in Table 10. Once the mesh yield stable and converged thrust results, the same mesh settings and operating conditions were applied to the two modified propeller designs. This ensured a consistent and unbiased comparison of aerodynamic performance across all configurations.

Data Parameters for Baseline Propeller Analysis	
Air Density (ρ)	$1.225 kg/m^3$
Rotational Speed (RPM)	$3808 rev/min$
Rotational Speed (ω)	$398.773 rad/sec$
Diameter of Propeller (D)	$0.220 m$
Freestream Velocity	$0 m/s$

Table 10: Data Parameters for Baseline Propeller Design

Table 11 presents the grid resolution details for the baseline propeller. Similarly to the validation phase, this propeller also employs six mesh densities, ranging from extra coarse to extra fine.

Type of Mesh	No. of Nodes	No. of Elements
Extra Coarse	84565	458109
Coarse	203591	1633272
Fine	374460	2017818
Mid Fine	596531	3222121
Fine	830275	4484734
Extra Fine	1040737	5615360

Table 11: Grid Resolution for Baseline Propeller Design

Table 12 presents the aerodynamic parameters obtained from CFD simulations for respective mesh resolutions. Using equations 7,8 and 9, the thrust and power coefficient was then calculated.

Type of Mesh	Thrust (N)	Torque (Nm)	C_T	C_P
Extra Coarse	0.95532	0.01434	0.08265	0.03543
Coarse	0.86249	0.01365	0.07461	0.03373
Mid	0.81214	0.01342	0.07026	0.03316
Mid Fine	0.72944	0.01330	0.06312	0.03286
Fine	0.68256	0.01310	0.05905	0.03237
Extra Fine	0.69834	0.01309	0.06042	0.03234

Table 12: Aerodynamic Parameters for Mesh Independence Study

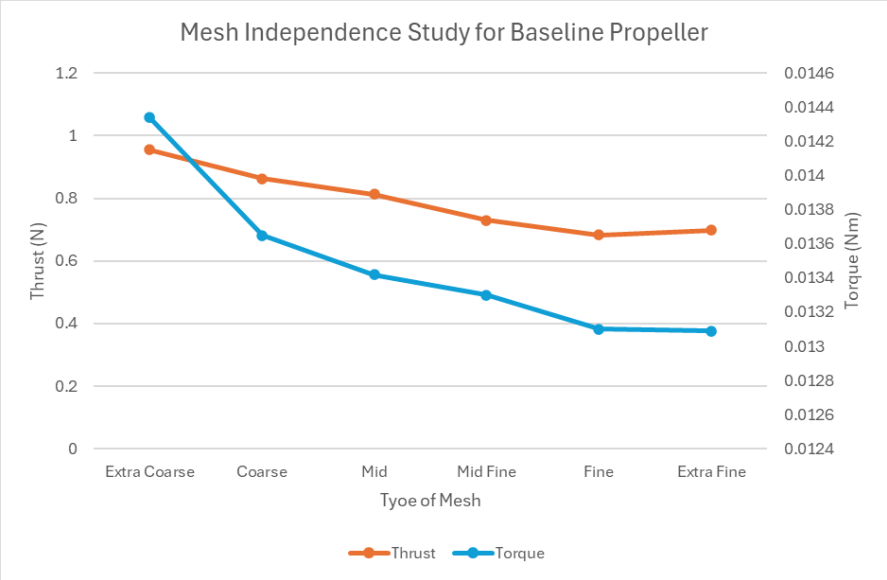

Figure 26: Thrust and Torque Convergence

Figure 26 shows the graphical results of the mesh independence study conducted on the baseline propeller, illustrating the convergence behaviour of thrust and torque across various mesh resolutions. From the graph, it can be observed that the thrust begins to stabilise around the fine mesh resolution, with negligible changes between the fine and extra fine meshes. Similarly, the torque values show minimal variation beyond the mid-fine to fine range. This indicates that further mesh refinement beyond the fine mesh offers negligible improvement in accuracy. Therefore, the fine mesh resolution is selected as the optimal mesh setting for all subsequent simulations propeller designs, ensuring consistent and mesh-independent results across all configurations.

4.2 MODIFICATION 1: SWEPT BACK PROPELLER BLADES

Figure 27 and 28 shows the first modification, which features a swept-back propeller blade design. This geometry was introduced by sweeping the blade tip rearward relative to the direction of rotation. The aim of this modification is to reduce induced drag and tip vortex strength, which are known to contribute to aerodynamic losses, particularly at the blade tips.

Hypothesis: Incorporating a swept-back tip will lead to an improvement in aerodynamic efficiency by enabling smoother airflow over the blade, thereby reducing vortex shedding at the tip and enhancing thrust generation while minimising power consumption.

This effect is well-implemented in fixed-wing and rotorcraft applications, where swept-back configurations have shown to delay flow separation and improve performance [16].

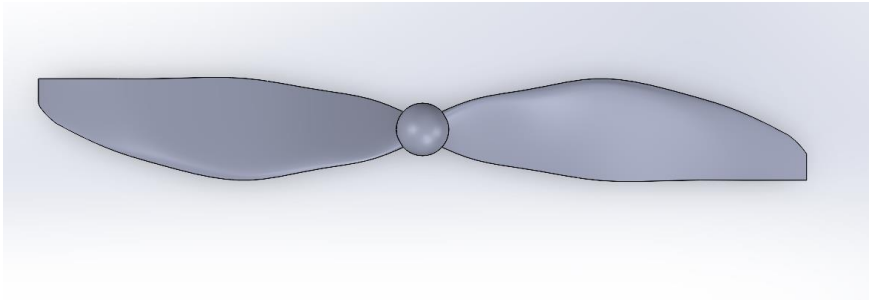

Figure 27: Swept Back Propeller (Top View)

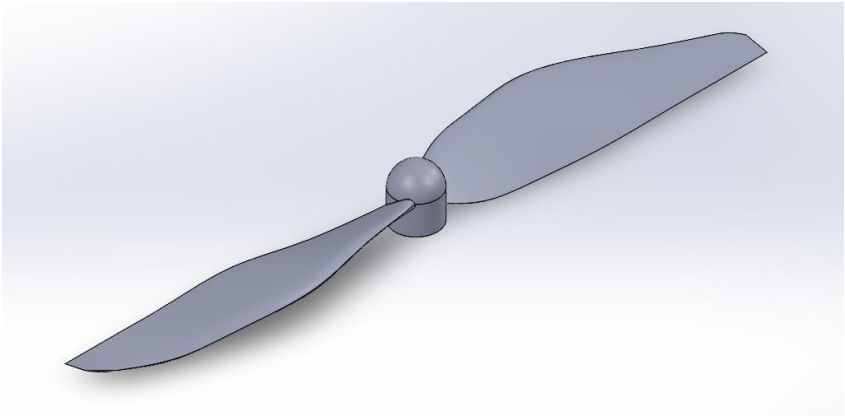

Figure 28: Swept Back Propeller (Isometric View)

The swept-back propeller was simulated using the same operating conditions listed in Table 10, and the 'fine' mesh resolution previously established for the baseline propeller. The corresponding CFD simulation results for this modified design are summarised in Table 13.

Propeller	Thrust	Torque	C_T	C_P
Swept Back	0.73676	0.01414	0.06374	0.03494

Table 13: Swept Back Propeller Simulation Results

4.3 MODIFICATION 2: DOWNWARD WINGTIPS

Figures 29 and 30 shows the second design modification, which incorporates a downward-facing winglet at the tip of each propeller blade. This feature was added to alter the flow direction at the blade tip and reduce the strength of trailing vortices, which are a common source of induced drag and energy loss in propeller operation.

Hypothesis: The implementation of a downward winglet will help redirect the tip flow downward, improving thrust efficiency by reducing vortex-induced flow separation and enhancing the pressure distribution across the blade span.

Winglets are widely used in fixed-wing aircraft and wind turbine applications to improve lift-to-drag ratio, and this concept is adapted here to assess its potential benefits for UAV propeller performance in static hover [14].

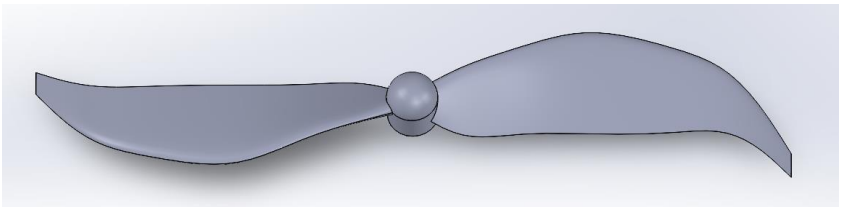

Figure 29: Downward Wingtips Propeller (Top View)

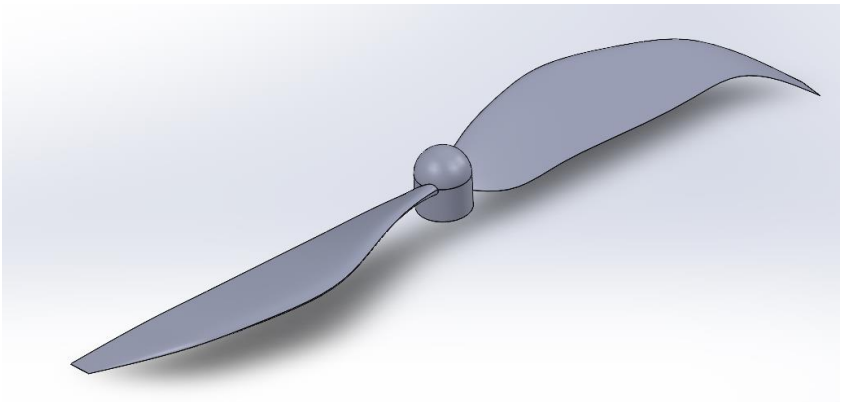

Figure 30: Downward Wingtips Propeller (Isometric View)

The downward wingtips propeller was simulated using the same operating conditions listed in Table 10, and the 'fine' mesh resolution previously established for the baseline propeller. The corresponding CFD simulation results for this modified design are summarised in Table 14.

Propeller	Thrust	Torque	C_T	C_P
Downward Winglet	0.68092	0.01236	0.05891	0.03054

Table 14: Downward Winglet Propeller Simulation Results

5 RESULTS AND ANALYSIS

Following the CFD simulations, key performance metrics—including thrust, torque, thrust coefficient, and power coefficient were evaluated to determine whether the added design features enhanced the hovering efficiency of the propeller blades. Table 15 provides a summary of the CFD simulation results, comparing thrust, torque, and thrust-to-torque ratio for the baseline, swept-back, and downward winglet propeller designs.

Propeller	**Thrust (N)**	**Torque (Nm)**	**Thrust to Torque Ratio**	C_T	C_P
Baseline	0.68256	0.01310	52.10382	0.05905	0.03237
Swept Back	0.73676	0.01414	52.10467	0.06374	0.03494
Downward Winglets	0.68092	0.01236	55.09061	0.05891	0.03054

Table 15: Summary of CFD results

From table 15, it can be observed that among the three configurations, the swept back propeller generates the highest thrust at 0.73676 N, slightly improving on the baseline's performance. However, it also requires the highest torque of 0.01414 Nm, resulting in a thrust-to-torque ratio nearly identical to the baseline at 52.10.

The downward winglet design, while producing a slightly lower thrust of 0.68092 N, achieves the highest thrust-to-torque ratio at 55.09, owing to its lower torque of 0.01236 Nm. This indicates a more efficient design, delivering relatively strong thrust with reduced power input.

Figure 31 illustrates a comparison graph between the thrust and power coefficient of the different propeller design. This comparison highlights how effectively each design converts rotational input into useful thrust.

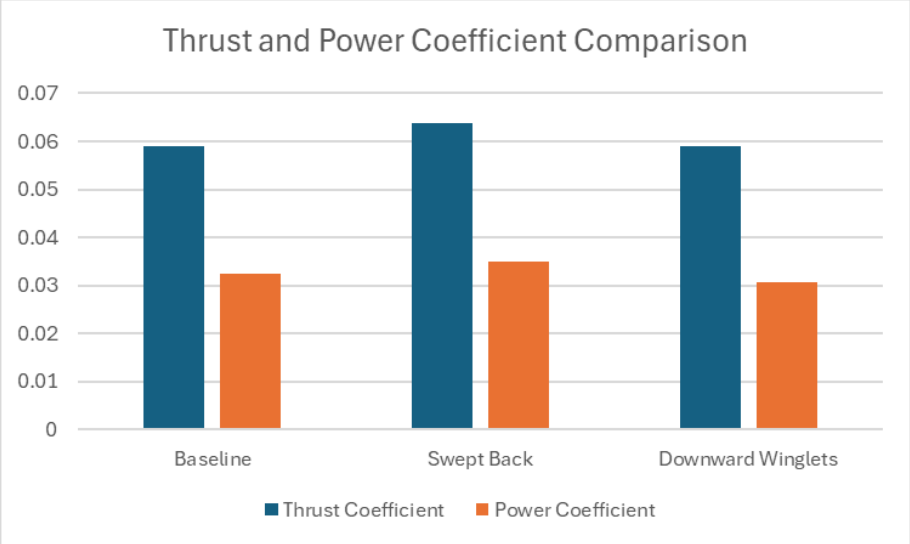

Figure 31: Thrust and Power Coefficient Comparison Graph

From Figure 31, it can be observed that the Swept Back propeller shows the highest values for both coefficients, suggesting strong aerodynamic performance but with a corresponding increase in energy demand. Meanwhile, the Downward Winglet design achieves a lower power

coefficient compared to the other two, indicating reduced energy consumption relative to thrust produced.

5.1 VELOCITY CONTOUR

To assess the aerodynamic behaviour of the different propeller designs, velocity contours were generated to visualise the flow field around the blades. These visualisations highlight key flow characteristics such as high-speed regions, acceleration over the blade surface, and areas prone to flow separation, all of which directly impact thrust production. Figures 32, 33, and 34 illustrate the velocity contours for the baseline, swept-back, and downward winglet propellers, respectively.

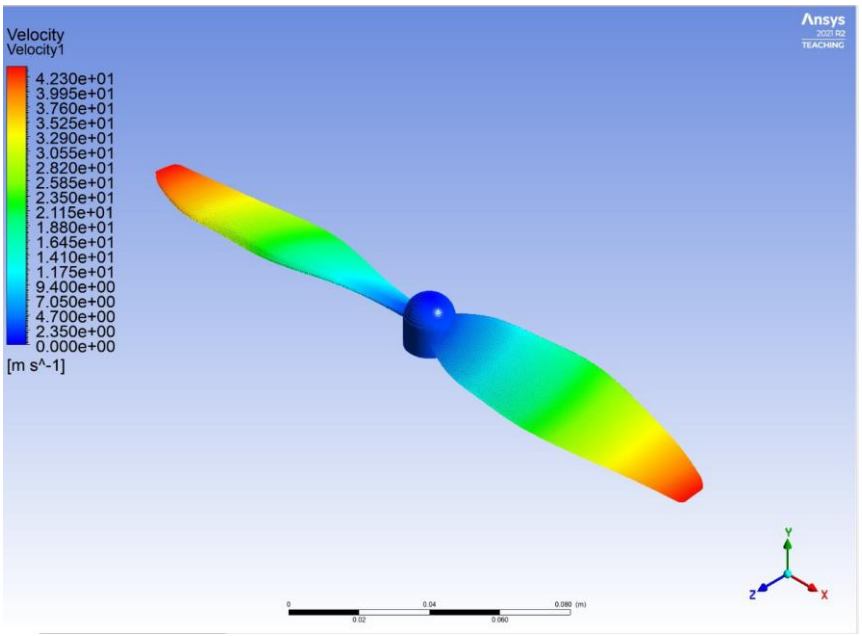

Figure 32: Velocity Contour of Baseline Propeller

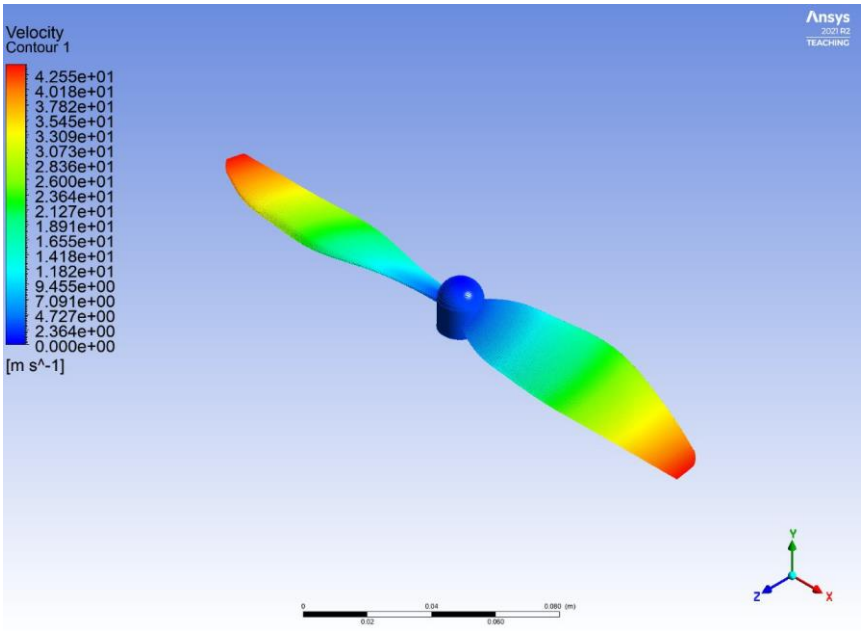

Figure 33: Velocity Contour of Swept Back Propeller

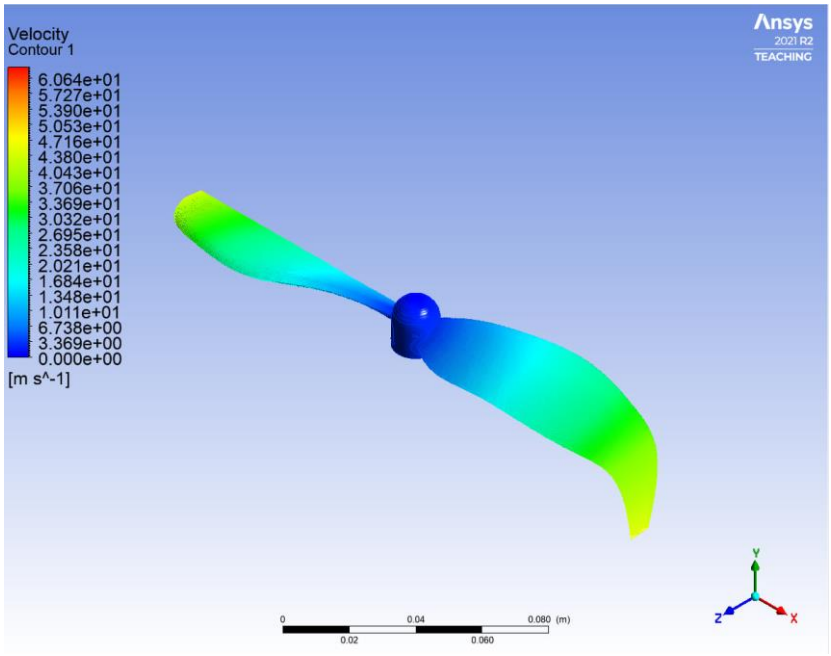

Figure 34: Velocity Contour of Downward Winglet Propeller

Comparing the velocity contours of the respective propeller, the velocity contours of the baseline, swept-back, and downward winglet propellers reveal distinct aerodynamic characteristics that influence their performance under static hovering conditions. The baseline propeller exhibits a typical velocity profile, with the highest airflow velocity concentrated near the blade tips, while the inner span generates significantly less thrust due to reduced flow acceleration.

In contrast, the swept back propeller shows a smoother and more evenly distributed velocity field along the blade span, with high-speed regions extending further inboard. This indicates more efficient blade utilisation and reduced aerodynamic loading at the tips, contributing to improved thrust generation.

The downward winglet propeller, although displaying similar peak tip velocities to the baseline, demonstrates enhanced flow redirection near the blade tips. The velocity contour suggests that the winglet weakens the tip vortex and helps manage the wake more effectively, resulting in better thrust-to-torque efficiency. Overall, the swept-back design improves thrust output, while the downward winglet offers aerodynamic efficiency through reduced energy loss.

To further examine the airflow behaviour around the propeller, a cross-sectional view in the xy-plane was generated to visualise the flow characteristics through the propeller disc.

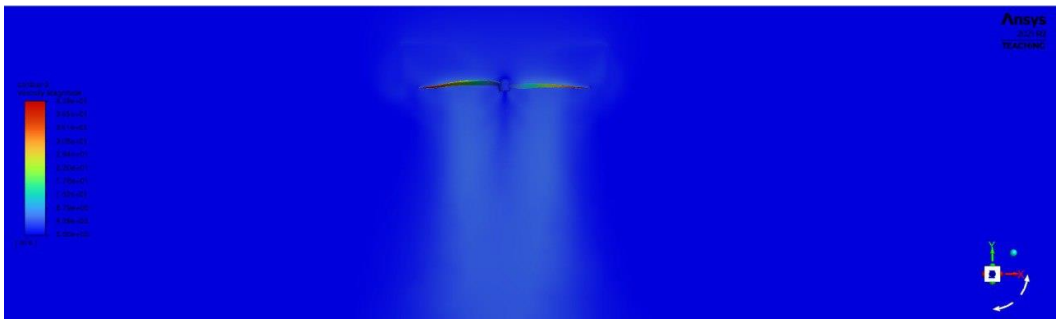

Figure 35: Cross-Sectional View of Baseline Propeller Velocity Contour

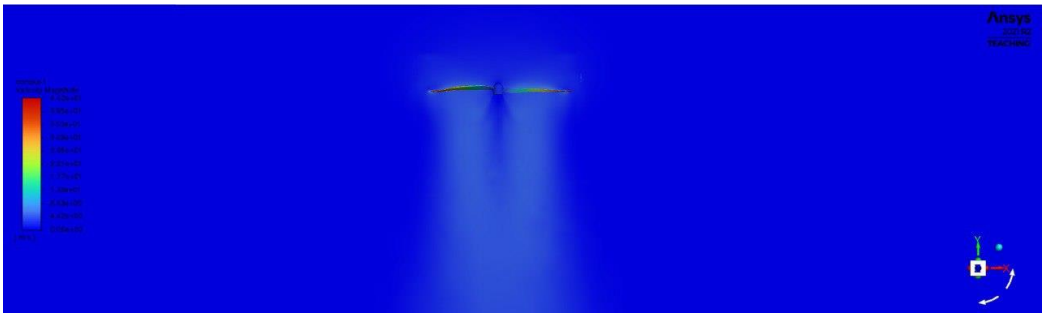

Figure 36: Cross-Sectional View of Swept Back Propeller Velocity Contour

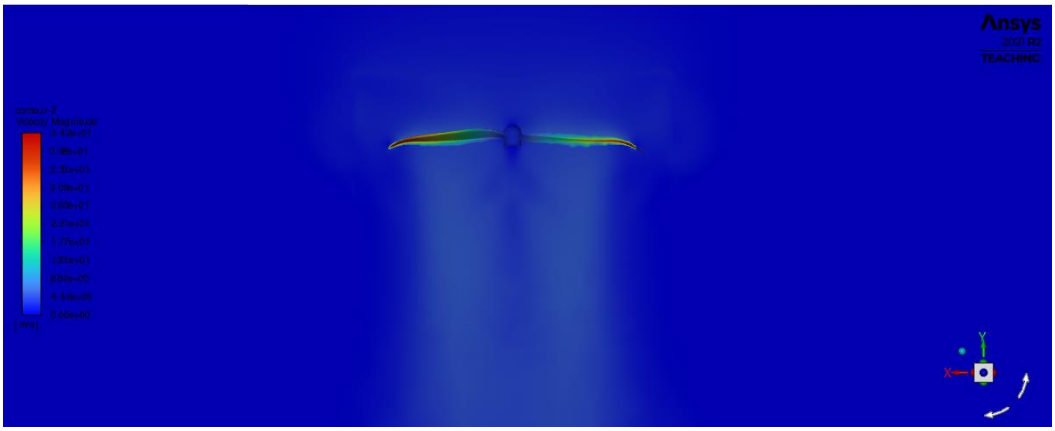

Figure 37: Cross-Sectional View of Downward Winglet Propeller Velocity Contour

Figures 35, 36, and 37 shows the cross-sectional velocity contours for the baseline, swept-back, and downward winglet propeller designs. These contours provide insight on their wake characteristics and aerodynamic performance.

From Figure 35 it is observed that the baseline propeller exhibits a relatively narrow and symmetric wake, with high-velocity flow concentrated along the central axis. While this indicates a focused thrust output, the rapid dissipation of velocity near the blade tips suggests potential energy losses due to strong tip vortices and less effective flow control.

In contrast, from Figure 36, it is shown that the swept-back propeller shows a more diffused wake, with high-speed airflow extending further outward from the centreline. This broader distribution implies better blade loading and improved suppression of tip vortices, contributing to enhanced thrust generation. The velocity field appears smoother and more stable, indicating that the swept-back geometry supports more efficient aerodynamic performance by delaying flow separation and reducing induced drag.

The downward winglet configuration presents the most uniform and well-distributed wake among the three designs. Referring to Figure 37, the velocity contour shows high-speed flow more evenly spread across the propeller span, with flow redirection evident at the blade tips. This suggests that the winglets effectively mitigate vortex formation and improve flow control, resulting in a more stable and efficient thrust output.

5.2 PRESSURE CONTOUR

Pressure contours were generated to visualise the pressure distribution across the blade surfaces. These contours reveal critical aerodynamic behaviours, such as regions of high and low pressure, and potential flow separation, all of which directly influence thrust generation and efficiency. Figures 38, 39, and 40 present the pressure contours for the baseline, swept back, and downward winglet propellers, respectively, highlighting how blade geometry affects pressure loading and overall aerodynamic performance.

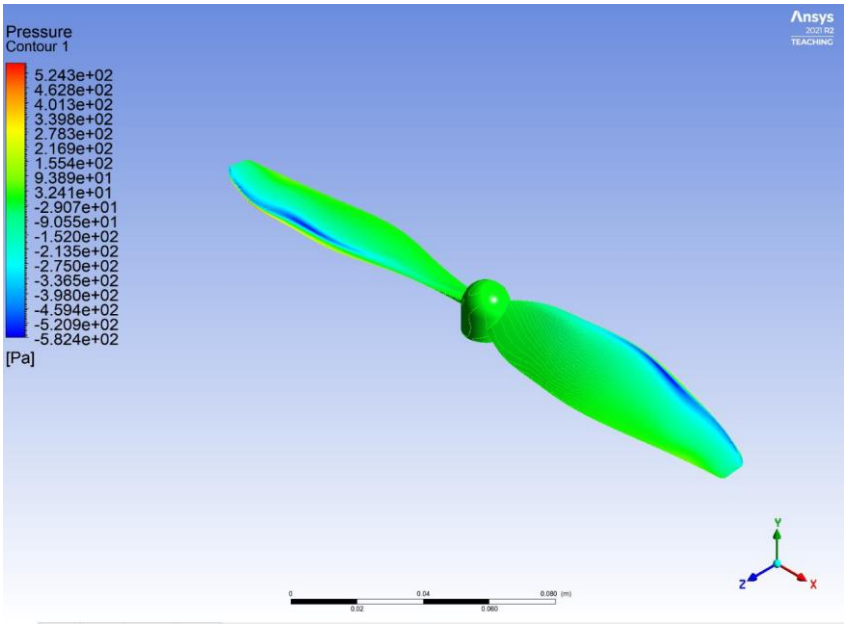

Figure 38: Pressure Contour of Baseline Propeller

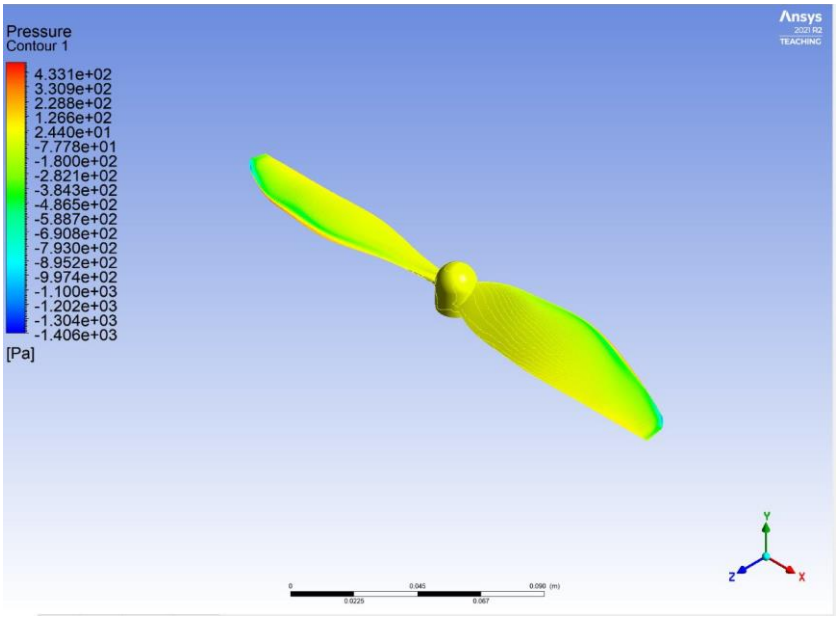

Figure 39: Pressure Contour of swept back propeller

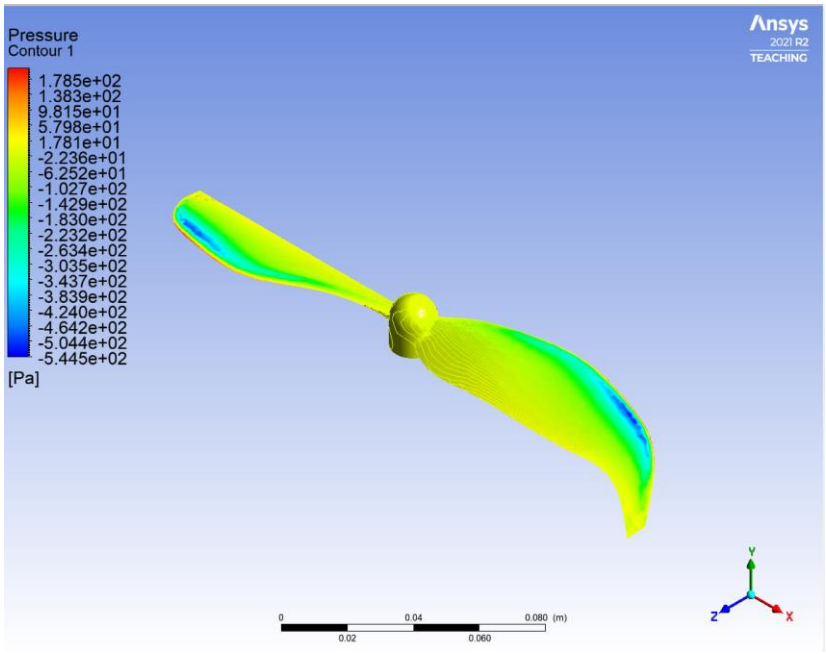

Figure 40: Pressure Contour of Downward Winglet Propeller

From figure 38, it shows that for the baseline propeller, high-pressure regions are concentrated on the leading surface near the blade roots, with low-pressure zones appearing on the suction side towards the tips. This pressure differential is responsible for thrust generation but also indicates that much of the aerodynamic load is localised near the tips, which can contribute to energy losses through strong tip vortices.

On the other hand, the swept-back propeller (Figure 39) displays a more pronounced and extended low-pressure region along the suction side, particularly further inboard along the blade span. This broader area of pressure drop suggests enhanced lift generation over a larger portion of the blade, improving overall thrust. Additionally, the pressure gradient appears smoother, which may help reduce flow separation and improve aerodynamic efficiency.

The downward winglet propeller (Figure 40) shows a more evenly distributed pressure field, especially at the blade tips. The winglet helps to redirect the flow, minimising abrupt pressure differences and potentially suppressing vortex formation. This results in a more balanced pressure distribution and improved pressure recovery near the trailing edge. Overall, the swept-back blade maximises thrust through stronger pressure differentials, while the downward winglet enhances efficiency by reducing tip losses and maintaining a smoother pressure profile.

To further investigate the airflow behaviour across the propeller disc, a pressure contour in the xz-plane was generated, allowing visualisation of pressure distribution. Figures 41, 42 and 43 shows the pressure contour of the baseline, swept back and downward winglet propeller respectively.

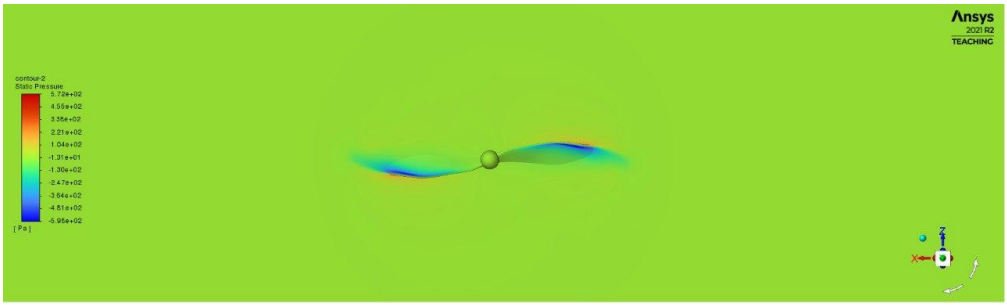

Figure 41: Top View Pressure Contour of Baseline Propeller

Figure 42: Top View Pressure Contour of Swept Back Propeller

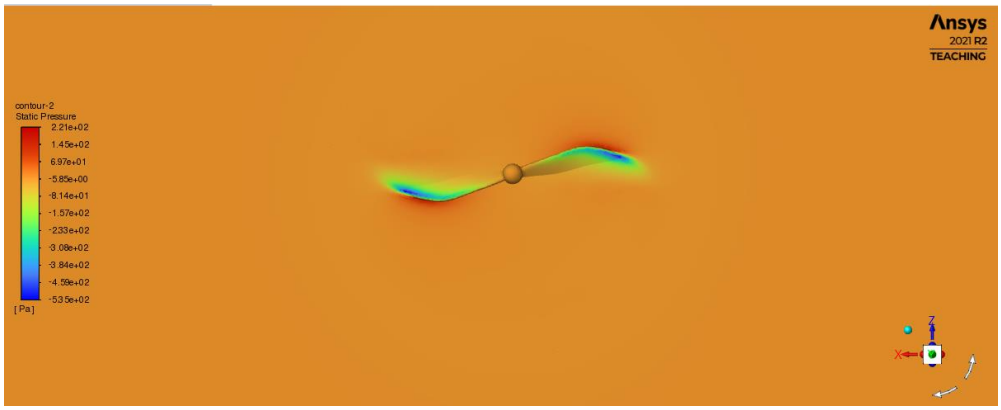

Figure 43: Top View Pressure Contour of Downward Winglet Propeller

From Figure 41, it can be observed that the baseline propeller exhibits a relatively concentrated pressure differential near the blade tips, with low-pressure regions forming below the propeller disc. However, the pressure spread appears narrow, indicating that much of the aerodynamic loading is localised at the outer blade span, which can lead to energy loss through strong tip vortices.

On the other hand, the swept-back propeller (Figure 42), displays a more expansive low-pressure region that stretches further radially inwards toward the hub. This indicates a broader area of effective pressure differential, which contributes to improved thrust distribution along the blade span. Additionally, the smoother and more continuous pressure contours suggest better pressure recovery and more efficient airflow control, which aligns with its improved thrust performance observed in CFD results.

Lastly, the downward winglet propeller (Figure 43) shows a balanced and symmetric pressure field, with pressure contours that suggest a smoother flow redirection around the blade tips.

The winglet helps contain and redirect the wake, reducing pressure loss at the tips. This leads to improved pressure uniformity behind the disc, which enhances thrust-to-torque efficiency. Overall, the cross-sectional pressure analysis highlights the aerodynamic benefits of both modifications: the swept-back blade enhances thrust through greater pressure differential.

5.3 Summary of Analysis

Based on the evaluation of the velocity and pressure contours across all three propeller designs, the swept-back propeller proves to be the most effective configuration for enhancing hovering efficiency. The velocity contours demonstrate a broader and more uniform high-speed flow along the blade span, particularly toward the tips, indicating enhanced aerodynamic loading and reduced energy losses. Similarly, the pressure contours reveal an extended low-pressure region on the suction side of the blade and smoother pressure gradients, both of which contribute to increased thrust generation and more stable flow attachment. These results support the first hypothesis: *Incorporating a swept-back tip will lead to an improvement in aerodynamic efficiency by enabling smoother airflow over the blade, thereby reducing vortex shedding at the tip and enhancing thrust generation while minimising power consumption.*

The downward winglet propeller, while producing slightly lower thrust than the swept-back configuration, exhibited a more symmetric and stabilised wake with better tip flow redirection. The pressure and velocity contours show improved pressure uniformity and reduced flow separation near the tips. This aligns with the second hypothesis: *The implementation of a downward winglet will help redirect the tip flow downward, improving thrust efficiency by reducing vortex-induced flow separation and enhancing the pressure distribution across the blade span.* Although it does not produce the highest thrust, the downward winglet design shows the highest thrust-to-torque ratio, validating its effectiveness in improving aerodynamic efficiency.

In conclusion, both modifications validate their respective hypotheses, with the swept-back blade optimising thrust generation and the downward winglet enhancing energy efficiency. However, for applications prioritising maximum thrust under static hover conditions, the swept-back design stands out as the preferred geometry.

6 CHALLENGES AND REFLECTION

One of the most significant challenges encountered during this project was the inherent limitation of using a steady-state MRF approach in accurately predicting the power coefficient. The MRF method simplifies the simulation by assuming a steady flow in the rotating frame, making it computationally efficient. However, it does not capture unsteady aerodynamic phenomena such as blade-wake interaction, vortex shedding, or dynamic stall, which are critical for precise torque and power predictions—especially under static hovering conditions. As a result, the MRF approach tends to overpredict power coefficient, introducing uncertainty when validating against experimental power data.

To address this limitation, the thrust coefficient was used as the primary validation metric, as it is less sensitive to these unsteady effects and more reliably captured by steady-state simulations. The CFD-predicted thrust coefficient values showed good validation with experimental results from the UIUC Propeller Database, confirming the model's validity in resolving key aerodynamic forces.

While power coefficient was still evaluated during the propeller design phase to assess the relative efficiency of different geometries, it was used primarily for comparative analysis rather than validation. This allowed the study to identify which designs provided better thrust-to-power ratios, while acknowledging the limitations in absolute power prediction. By taking this approach, the project ensured both the credibility of the CFD validation and the relevance of the design performance analysis, without compromising on computational practicality.

7 FUTURE WORK

To build upon the findings of this study, future work could explore the use of transient simulation techniques, such as Sliding Mesh or Large Eddy Simulation (LES), to capture unsteady aerodynamic phenomena like vortex shedding, blade-wake interaction, and dynamic stall. These advanced methods could provide more accurate predictions of power coefficient and unsteady forces, although they would require significantly higher computational resources.

Further optimisation may also include the development of hybrid blade geometries that combine both swept-back features and downward winglets, potentially leveraging the advantages of both configurations—enhancing thrust while minimising energy losses. Additionally, parametric studies using design of experiments (DOE) or response surface methods could be employed to systematically explore the effects of twist, chord distribution, and airfoil selection.

For implementation, prototype fabrication and wind tunnel testing of the optimised propellers would provide essential experimental validation and help assess manufacturability and performance in real-world scenarios. Integrating the optimised propeller into a working UAV platform and evaluating its performance in actual flight conditions—including hover, forward flight, and transitional manoeuvres—would further confirm its effectiveness.

Lastly, further studies could consider the influence of material flexibility, blade deformation at high RPMs, and Reynolds number variation, particularly for missions involving payload delivery or extended hover durations. Evaluating noise characteristics and their impact on propeller design for urban UAV operations could also be a valuable area of exploration, especially for use in emergency response or medical delivery applications where low acoustic signatures are preferred.

8 CONCLUSION

This study successfully demonstrated how geometric modifications to a quadcopter propeller can significantly influence aerodynamic performance under hovering conditions, using CFD with the MRF approach. The project was carried out in two key phases: validation and design exploration.

In the validation phase, simulations of two APC propellers (10x7” and 8x3.8”) were conducted and compared against wind tunnel data from the UIUC Propeller Database. A mesh independence study was performed to ensure reliable results, and the thrust coefficient was used as the primary validation metric. The validation with experimental data confirmed the accuracy and credibility of the CFD model using the MRF method, despite minor overpredictions in power coefficient due to the steady-state limitations of the approach.

In the design research phase, two geometric modifications—a swept-back blade and a downward winglet—were introduced and evaluated against the validated baseline. The swept-back propeller produced the highest thrust, along with smoother velocity profiles and more favourable pressure distributions, confirming its effectiveness in reducing tip vortex intensity and improving lift. The downward winglet, although slightly lower in absolute thrust, achieved the highest thrust-to-torque ratio, supporting its role in improving aerodynamic efficiency through better flow control and reduced induced drag.

Both designs demonstrated measurable aerodynamic benefits. The swept-back propeller is best suited for applications demanding maximum thrust under static hover conditions, as it offers better lift generation and more efficient energy conversion. The downward winglet propeller, meanwhile, is better suited for missions prioritising energy efficiency and stable wake behaviour.

In conclusion, this research validates the MRF-based CFD framework as a reliable tool for UAV propeller development. The study provides practical insight into how specific geometric features influence aerodynamic performance and establishes a strong foundation for future design optimisation and experimental validation in UAV propulsion systems.

9 REFERENCES

[1] Mohsan, S. A. H., Othman, N. Q. H., Li, Y., Alsharif, M. H., & Khan, M. A. (2023). Unmanned aerial vehicles (UAVs): Practical aspects, applications, open challenges, security issues, and future trends. *Intelligent Service Robotics*, 16, 109–137. https://doi.org/10.1007/s11370-022-00452-4

[2] Statista. (n.d.). *Global market value of Unmanned Aerial Vehicles (UAVs) in 2018 and 2029 (in billion U.S. dollars).* Retrieved February 24, 2025, from https://www.statista.com/statistics/1052890/global-uav-market-value/

[3] Drone Pilot Ground School. (n.d.). *Drone types and uses: A comprehensive guide for drone pilots.* Retrieved February 24, 2025, from https://www.dronepilotgroundschool.com/drone-types/

[4] ResearchGate. (2024). *Optimization of quadcopter propeller aerodynamics using blade element and vortex theory.* Retrieved from https://www.researchgate.net/publication/385676002_Optimization_of_Quadcopter_Propeller_Aerodynamics_Using_Blade_Element_and_Vortex_Theory

[5] Mohd Sani, F., Mohamad Zin, A. A. I., Mohd Nor, E., Kamarudin, N. D., & Makhtar, S. N. (2024). *Comparison of VTOL UAV battery level for propeller faulty classification model*. JOIV: International Journal on Informatics Visualization, 8(2), 717–723. https://doi.org/10.62527/joiv.8.2.2177

[6] Yang, X., Shen, H., Wang, J., Zhou, D., & Zhang, Y. (2021). *Review of propeller modeling and applications for multirotor UAVs.* Aerospace, 8(11), 349. https://doi.org/10.3390/aerospace8110349

[7] Pilotfriend. (n.d.). *Aircraft propellers – how they work*. Retrieved from http://www.pilotfriend.com/training/flight_training/fxd_wing/props.htm

[8] NASA/ERAU. (n.d.). *Propellers*. In *Introduction to Aerospace Flight Vehicles*. EaglePubs. Retrieved from https://eaglepubs.erau.edu/introductiontoaerospaceflightvehicles/chapter/propellers/

[9] Aerodynamics for Students. (n.d.). *Blade element propeller theory*. Retrieved from https://www.aerodynamics4students.com/propulsion/blade-element-propeller-theory.php

[10] Southern Wings Flight Training. (n.d.). *Aircraft Propeller Basics*. Retrieved from https://www.southernwings.co.nz/aircraft-propeller-basics/

[11] Learn to Fly Blog. (n.d.). *Aerodynamics: Propeller Basics*. Retrieved from https://learntoflyblog.com/aerodynamics-propeller-basics/

[12] Bergmann, O., et al. (2021). *Aerodynamic analysis of swept propeller with BET and RANS*. ResearchGate. Retrieved from https://www.researchgate.net/publication/354282279

[13] Dinham, J., et al. (2018). *A review of propeller modelling techniques in UAVs*. *Aerospace Science and Technology*, 81, 129–141. https://www.sciencedirect.com/science/article/pii/S1270963818319473

[14] Aviation Stack Exchange. (n.d.). *Why are downward-pointing winglets more efficient?* Retrieved from https://aviation.stackexchange.com/questions/39769/

[15] Basset, A., & Cadoux, F. (2019). *Effect of disk angle-of-attack on the performance of propellers for small UAVs*. *Aerospace Science and Technology*, 91, 575–583. https://doi.org/10.1016/j.ast.2019.05.047

[16] Andre, T., et al. (2017). *3D CFD Simulation and Experimental Validation of Small APC Slow Flyer Propeller Blade*. ResearchGate. https://www.researchgate.net/publication/314033938

[17] CFD Source. (n.d.). *CFD analysis of propellers*. Retrieved from https://www.cfdsource.com/ShowBlog/cfd-analysis-of-propellers/

[18] Resolved Analytics. (n.d.). *CFD for marine propulsion*. Retrieved from https://www.resolvedanalytics.com/cfd-applications/cfd-for-marine-propulsion

[19] Wärtsilä. (n.d.). *6 helpful facts about CFD that might surprise you*. Retrieved from https://www.wartsila.com/insights/article/computational-fluid-dynamics-6-helpful-facts-about-cfd-that-might-surprise-you

[20] Menter, F. R. (1994). *Two-equation eddy-viscosity turbulence models for engineering applications*. *AIAA Journal*, 32(8), 1598–1605. https://doi.org/10.2514/3.12149

[21] UIUC. (n.d.). *UIUC Propeller Data Site*. Retrieved from https://m-selig.ae.illinois.edu/props/propDB.html

[22] Maulana, A., et al. (2015). *Computational analysis of marine-propeller performance using transition-sensitive turbulence modeling*. ResearchGate. https://www.researchgate.net/publication/277520276

[23] APC Propellers. (n.d.). *About APC*. Retrieved from https://www.apcprop.com/about/

[24] Wang, Z., et al. (2019). *Modeling and performance simulation of a micro turbojet engine using Flownex*. ResearchGate. https://www.researchgate.net/publication/335154510

[25] Murayama, M., et al. (1997). *Effects of leading-edge separation vortex of flexible structure delta wing on its aerodynamic characteristics*. ResearchGate. https://www.researchgate.net/publication/245395908

[26] Rezaeiha, A., et al. (2017). *Towards accurate CFD simulations of vertical axis wind turbines at different tip speed ratios and solidities*. ResearchGate. https://www.researchgate.net/publication/321490737